CAAP Final Report

Date of Report: March 9, 2023

Prepared for: *U.S. DOT Pipeline and Hazardous Materials Safety Administration*

Contract Number: 693JK31850002CAAP

Project Title: **Smart Fluids for Detecting Internal Corrosion Locations in Oil and Gas Pipeline**

Prepared by: Anne Co, The Ohio State University

Contact Information: Anne Co, co.5@osu.edu

Smart Fluids for Detecting Internal Corrosion Locations in Oil and Gas Pipeline

TABLE OF CONTENTS

TABLE OF FIGURES

Executive Summary

The goal of this proposed work is to demonstrate a chemical tag selective to Fe^{2+} and Fe^{3+} for detecting internal corrosion of a gas pipelines. We have successfully identified an Fe^{2+} dye, FerroFarRed, that is highly selective to Fe^{2+}, very stable across a wide range of pH range, and commercially available. The Fe^{3+} dye, however, is not commercially available. We have therefore set out to synthesize reported dye molecules that are selectively to Fe^{3+}. These are the (1) (E)-N-(1H-benzo[d]imidazol-2-yl)-1-(quinolin-2-yl)methanimine (BIM), (2) N-[Tris(N-ethyl-1,8-naphthalimide)]amine (NET), and (3) 2-(2-((anthracen-9-ylmethyl)amino)ethyl)-3',6'-bis(diethylamino)spiro[isoindoline-1,9'-xanthen]-3-one (AMAE-RhB).

Our synthesized dye closely resembles those of the literature report in terms of their chemical characteristics identified using NMR, IR and UV. However, upon multiple attempts to measure their selectivity towards Fe^{3+}, our results deviated from the literature. As it turns out, these dyes are pH sensitive, and therefore induces a change in the signal upon mixing with Fe^{3+} solution. We have confirmed their pH sensitivity by preparing the Fe^{3+} solution in a buffered solution and in this work we have unequivocally proved the pH sensitive nature of the Fe^{3+} dye investigated in this work. Herein we conclude that the BIM and AMAE-RhB dye are pH sensitive, with a sharp increase in intensity between pH 2 to 4, with the AMAE-RhB exhibiting a slightly narrower pH sensitive range compared to the BIM dye. Future work on the effect of pressure, flow and temperature on the stability of the Fe^{2+}-FerroFarRed and the pH sensitive dyes would be interesting in demonstrating their applicability in quantifying internal corrosion and local pH along the pipeline.

Educational goals:

Several students and postdocs were involved in this project since its inception. The first two postdocs, Jose Lorie Lopez and Pamela Smecellato, were both crucial in getting the project started by identifying key dye molecules, setting up the equipment for synthesizing and characterizing dye molecules, and for corrosion testing, as well as training the graduate students who participated in this project. Both Jose and Pamela were highly involved in the discussions with our industrial collaborator at DNVGL to identify relevant experimental test conditions that simulates pipeline conditions. Our team has been in close collaboration and have regular discussions with DNVGL before the pandemic. Both Jose and Pamela continued to assist and support the student throughout the project. Jose Lorie Lopez is currently a Research Scientist at OSU and Pamela Smecellato has moved to Israel and is currently employed at 3DBatteries at Rohovot, Israel. The graduate student involved in this project is Ariel Mendoza. With the support of this PHMSA project, Ariel had

successfully completed and defended his MSc thesis. The bulk of this report is based on Ariel's work towards his MSc thesis. Ariel is currently completing his PhD degree focusing on the synthesis of ion conducting materials. In addition, Angie Huggins, a former OSU student and a postdoctoral fellow with DNVGL at the time, was highly involved with this project during its inception. Angie is now gainfully employed by DNVGL.

Due to the disruptions from the pandemic. The postdocs and students who worked on this PHMSA project participated mostly in virtual symposiums organized by the Electrochemical Society. Journal publications based on the results from this work is in preparation. Ariel Mendoza's MSc thesis is published and available for the public to download from the Ohiolink (https://etd.ohiolink.edu/acprod/odb_etd/etd/r/1501/10?clear=10&p10_accession_num=osu1668516987924133). No patent application was submitted for this work based on our initial agreement with DNVGL. Due to the impact by the pandemic, pressure and flow tests were not conducted.

Student / postdoc	**Current position**
Jose Lorie Lopez	Research Scientist at OSU
Pamela Smecellato	Research Scientist, 3DBattery, Israel
Angie Huggins	Currently employed by DNVGL
Ariel Mendoza	Graduated with an MSc with PHMSA support. Currently pursuing his PhD in Chemistry at OSU.

1 Project Overview

1.1 Introduction

According to the PHMSA incident database, between 1998-2017, internal corrosion contributed approximately 12% of the incidents on transmission pipelines. Internal corrosion is caused by the accumulation of water in certain locations along the pipeline and the effect of impurities in the hydrocarbon being transported. For natural gas, the impurities include CO_2, O_2, and H_2S. The presence of bacteria can exacerbate the internal corrosion. The focus of this proposal is on natural gas pipelines, although the methodology can be applied to liquid hydrocarbon lines. Generally, three approaches are used by pipeline companies to monitor internal corrosion of natural gas pipelines:

- Pigging: Smart pigs (also called inline inspection, ILI, devices) are used at certain intervals to measure changes in wall thickness and other defects. ILI devices provide information on corrosion defects using ultrasonic and magnetic flux leakage sensors. However, these devices have several limitations: (i) they can only be used at high gas pressures to ensure coupling between the sensors and the pipe wall; (ii) many pipelines have severe bends, changes in cross sections, or intervening valve bodies that restrict the use of ILI devices; (iii) aligning a series of ILI readings to determine whether a corrosion defect is actively growing is difficult, and (iv) the time interval between ILI runs are too long to assess risks in between runs. Cleaning pigs are not outfitted with thickness sensors, but may have position sensors to determine their location if they are stuck. They are used to clear accumulated debris in the pipelines. The debris could be collected at the other end from launch point and analyzed to determine whether corrosive conditions exist, but their location is unknown.

- Direct Assessment: For those pipelines that cannot be inspected by pigging, procedures to assess internal corrosion possibility, called Internal Corrosion Direct Assessment (ICDA), have been developed. These rely on a combination of flow modeling and excavation of selected sites to determine whether corrosion conditions exist. There are many uncertainties in conducting ICDA and the resultant assessments. Additionally, excavation of identified sites can be prohibitively expensive.

- Fixed Probes and coupons: Fixed probes based on resistance tomography, electrochemical impedance, etc. have been deployed. Additionally, coupons are inserted at different locations and extracted to analyze conditions that could lead to internal corrosion. These fixed probes often miss

important locations where internal corrosion may occur and are not desirable because they require penetration of the pressure boundary.

1.1.1 Mobile Sensors in Pipelines

An alternative approach to monitoring internal corrosion is to insert mobile sensors that can move along the gas stream and detect locations of water accumulation. Previous projects conducted by co-PI Sridhar and follow-on projects conducted at DNV GL focused on thin film sensors mounted on a ball or on a cleaning pig that could move along the gas stream inside the pipeline. In this type of sensor, shown in Figure 1, the thin film interdigitated sensor is mounted on depressions on the O.D. of the ball and connected to data acquisition system and communication device inside the ball. Since this is relatively inexpensive, many sensors can be sent in the pipeline to improve spatial resolution of detection. A later evolution of the ball sensor was a sensor tethered to a cleaning pig (Figure 1).

Figure 1.1. Examples of ball sensors that can move along the gas stream

This type of sensor, while overcoming some of the limitations of ILI devices and fixed probes, had many limitations: (1) it missed some locations of corrosion, especially the top of the line corrosion found on the upper part of the pipelines in wet natural gas systems; (2) it was not mechanically robust; (3) it detected the water hold up, but not the corrosion of the steel pipe; and (4) the free flowing sensor got stuck at some locations, such as circumferential welds.

1.1.2 Smart Fluid Approach

We propose a radically new approach to detecting internal corrosion. This involves injecting tag chemicals in the gas stream that can bind to dissolved ferrous (Fe^{2+}) and ferric ions (Fe^{3+}) resulting from corrosion that can subsequently be picked up by an optical sensor attached to a cleaning pig with position detection sensors (Figure 2).

Essentially, we intend to make the fluid flowing in the pipeline "smart". The tag chemicals can be made to fluoresce or phosphoresce when bound to the ferrous ion (Fe^{2+}) so that a charge coupled device (CCD) camera can detect a signal. The intensity of the fluorescence may be related to the concentration of ferrous ions present and therefore indicate the corrosivity of the site and the presence of pooled water. Cleaning pigs are routinely used in pipelines and some of them have location sensors to ensure that they can be located, if stuck. By placing the camera well ahead of the pig face, the cleaned debris will not interfere with the signal. The cleaning pig has location information that can be correlated to the camera reading. This approach has many advantages: (1) there is no concern about hold up of the sensor at any pipeline features and the mechanical fragility of the sensor is not an issue; (2) since the tag chemicals attach to dissolved ferrous and ferric ions, the detection is sensitive to the extent of internal corrosion and not just water hold up; (3) the tags can also be combined with organic inhibitor molecules making mitigation a possibility. The technology is relatively inexpensive and uses routine equipment, such as cleaning pigs.

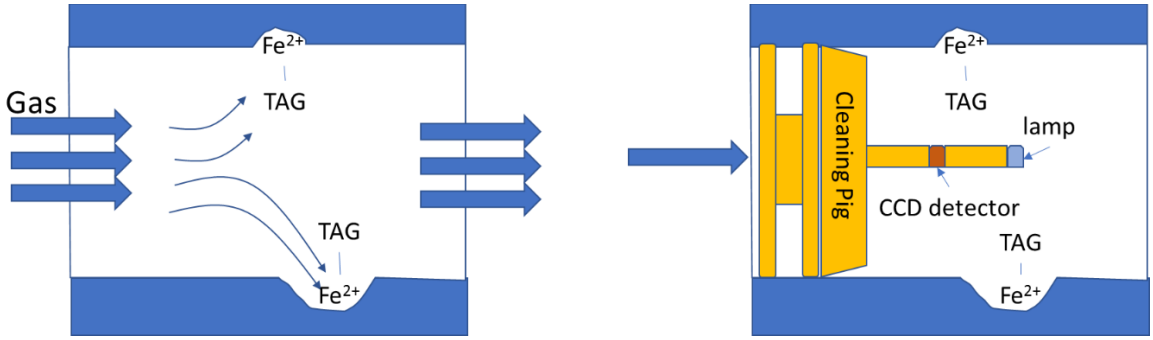

Figure 1.2. Smart fluid concept

The use of tag chemicals to indicate the presence of dissolved ferrous and ferric ions in pipes is novel. Other types of moving internal corrosion sensors have relied on detecting

the presence of moisture (through conductivity measurements). However, these sensors have not shown to be reliable. The detection of pH changes due to corrosion has been suggested, but pH changes may not be sensitive, especially if acidic gases are involved. Detection of ferrous ions may be quantitative.

Detecting internal corrosion in non-intrusive manner has always been a challenge. This method will enable a stepwise testing of a new method that uses existing facilities and equipment in a non-intrusive manner.

1.2 Project Objectives

The overall objective of the proposed research is to demonstrate the use of a tag chemical flowed along with the gas stream in monitoring internal corrosion of a gas pipelines.

1.3 Project Approach

The overall project is sectioned into the following tasks.

Task 1: Selection of Tags and Application Parameters

In this task, several commercially available and literature reported chemical tags known to complex with Fe^{2+} and Fe^{3+} selectively was identified. The idea is to down select candidate chemical tags, or dye molecules, that will selectively bind to Fe^{2+} and Fe^{3+}, respectively, providing a distinct fluorescence or phosphorescence signature. Chemical tags do not need to be molecular, they could also potentially be a nanoparticle, for example quantum dots, that has the desired selectivity, excitation and emission wavelengths. The down selection criteria identified includes (1) binding selectivity towards Fe^{2+} or Fe^{3+}, (2) excitation and fluorescence range, as this will define the type of lamp required (e.g. equipping the PIG with a tungsten lamp will be ideal). We anticipate the complex to be excited between 4325 and 500 nm and the fluorescence emissions detected between 500 to 800 nm. (3) temperature stable and (4) pH stable. Other considerations also include the reaction time required to reach optimum emission and the lifetime of the complex. Details regarding the specific tags selected will be described in later section of this report.

Task 2: Tests in High Pressure

In this task, the down selected tags were planned to be tested in an aqueous solution exposed to high pressure methane or CO_2 in an autoclave. The initial planned experiments will first investigate the stability of the Fe^{2+} and Fe^{3+} complex under high pressure by introducing the

chemical tag to a known Fe^{2+} and Fe^{3+} concentration, followed by the same experiments on exposed corroding steel. The tests were initially planned to be conducted at the high-pressure laboratory in DNV GL by the OSU student which will be confirmed with fluorescence measurement of the mixture to determine the concentration of Fe^{2+} or Fe^{3+} in solution using methods developed at OSU.

Task 3: Tests under flow conditions

The initial proposal includes a flow loop test to be conducted at DNV GL with pipes that can be adjusted to have several inclination angles to promote water hold up under a gas stream. Tag chemicals will be introduced with a gas stream, followed by a tethered optical detector. Between the pandemic and factors beyond this project, the initial flow loop was dismantled. During our midterm review, we proposed to redefine the scope of the project by removing this task or to utilize a smaller effort to simulate flow to detect Fe species from the corrosion of a steel coupon.

Task 4 Pathways for practical implementation

Given additional resources and time. This is a very exciting and promising project. Our partners at DNV GL have planned to identify pathways and industrial partners for practical implementation of the smart fluid concept. The implementation may begin with discussions with members of PRCI and associated inspection vendors. Preliminary discussions at the PRCI Research forum have indicated such interest.

2 Experimental

2.1 Materials

Three dyes were synthesized in this work. They are (E)-N-(1H-benzo[d]imidazol-2-yl)-1-(quinolin-2-yl)methanimine (BIM), N-[Tris(N-ethyl-1,8-naphthalimide)]amine (NET), and 2-(2-((anthracen-9-ylmethyl)amino)ethyl)-3',6'-bis(diethylamino)spiro[isoindoline-1,9'-xanthen]-3-one (AMAE-RhB). Chemicals used for the synthesis of BIM, NET, and AMAE-RHB are described in Sections 2.3-2.5. These chemicals were mostly used as received, unless specified in the description.

Salt solutions containing metal cations used in this work were prepared from the following salts: $K_3(Fe(CN)_6)$ (J.T. Baker, 99.5%), $Fe(NH_4)_2(SO_4)_2 \cdot 6H_2O$ (Mallinckrodt Pharma., 99.9%) , $Zn(C_2H_3O_2)_2 \cdot 2H_2O$ (Sigma-Aldrich, ≥98%), KCl (Sigma-Aldrich, ≥99.9%), $AlCl_3$ (Spectrum Chemical Mfg. Corp., ≥99.0%), $Cr(NO_3)_3 \cdot 9H_2O$ (J.T. Baker, 99.0%), $Mn(C_2H_3O_2)_2$ (Sigma-Aldrich, 98%), $CoCl_2 \cdot 6H_2O$ (Sigma-Aldrich, 98%), CuCl (J.T. Baker, 97.5%), $CuCl_2 \cdot 2H_2O$ (J.T. Baker, 99.8%), $NaNO_2$ (Sigma-Aldrich, ReagentPlus grade), NaCl (Fisher Chemical, 99.7%), $FeSO_3$ (Pfaltz & Bauer Inc., 98%), $NiCl_2 \cdot H_2O$ (Sigma-Aldrich, 99.95%), $CaCl_2 \cdot 2H_2O$ (Fisher Chemical, 100.0%), $Fe(NO_3)_3 \cdot 9H2O$ (J.T. Baker, 99.4%), and $FeCl_3$ (Sigma-Aldrich, ≥99.99%). Stock solutions were prepared in de-ionized water (Millipore,2 ppb, 18 MOhm). Specific concentrations of the prepared solutions are described in Section 2.6.

2.2 Instrumentation

2.2.1 Infrared spectra were collected using an Agilent Cary 630 FTIR spectrometer using a single reflection diamond ATR module in the 4000-650 cm^{-1} range. The instrument uses a dTGS detector and has a maximum spectral resolution of 2 cm^{-1}. FTIR spectra were collected at room temperature. Solid samples were loaded directly onto ATR crystal.

2.2.2 Ultra-Violet/Visible absorption spectra were collected using an Agilent Cary 5000 UV-Vis spectrophotometer using a tungsten halogen lamp and a deuterium arc lamp as sources for the visible and ultra-violet light ranges, respectively. The instrument uses a PbSmart PbS/PMT detector. Quartz cuvettes of 1 cm path length were used for during testing. A wavelength range of 250-650 nm was used to collect the spectrum at room temperature. Details of sample preparation are described in section 2.5.2.

2.2.3 ESI mass spectra were recorded using a Bruker Impact II UHR-QqTOF (Ultra-High-Resolution Quadrupole-quadrupole-Time-Of-Flight) mass spectrometer with an ESI source used in MS mode. All samples tested using LC-MS were dissolved in anhydrous ethanol (200 proof, Decon Labs).

2.2.4 ^{1}H NMR spectra were collected using a Bruker Avance III 400 MHz spectrometer using a 5 mm BBFO probe with Z gradient. NMR samples were prepared using 1 mg of solid dissolved in 0.6 mL of deuterated solvent.

2.2.5 All fluorescence spectra were collected using a Horiba Fluorolog-3 fluorimeter using a xenon arc lamp and an R928P PMT detector. Excitation wavelength and emission wavelengths collected, as well as details of sample preparation are described in Section 2.5.

2.2.6 A Fisher Scientific Accumet Excel XL20 pH conductivity meter was used to measure solution pH using an Orion 9102DJWP double junction pH probe.

2.3 Preparation of (E)-N-(1H-benzo[d]imidazol-2-yl)-1-(quinolin-2-yl)methanimine (BIM)

Synthesis of L_1. 2-aminobenzimidazole (400 mg, 3 mmol, Alfa Aesar, 97%) and quinoline 2-carboxaldehyde (471 mg, 3mmol, Alfa Aesar, 97%) were dissolved in 20 mL of anhydrous methanol (ChemProducts, >99.8%). Approximately 2 drops of glacial acetic acid (Sigma Aldrich, ACS grade) were added to the solution. Approximately 10 molecular sieves were added, and the solution was refluxed for 48 hours. Once a visible precipitate was formed, the reaction flask was cooled to room temperature. The contents of the reaction flask were added to a beaker and heated, allowing excess methanol to evaporate. Excess cold ultrapure deionized water (18.2 MΩ, Milli-Q system, Advantage A10) was added to the solution, which allowed for the formation of a precipitate. The precipitate was collected through filtration and washed with ice-cold deionized water to isolate L_1.

Synthesis of L_2. 2-aminobenzimidazole (400 mg, 3 mmol) and quinoline 2-carboxaldehyde (471 mg, 3mmol) were dissolved in 30 mL of methanol. Approximately 3 drops of acetic acid were added to the solution. Approximately 20 molecular sieves were added, and the solution was refluxed for 48 hours. Once a visible precipitate was formed, the reaction flask was cooled to room temperature and the precipitate was collected through filtration. The resulting supernatant was then heated to allow for excess methanol to evaporate. Excess ice-cold ultrapure deionized water was added to the supernatant, which allowed for the formation of a precipitate. The precipitate was collected through filtration and washed with ice-cold deionized water to isolate L_2. The resulting supernatant was refrigerated overnight. The supernatant was filtered once more to isolate a third

precipitate.

Synthesis of L_3. 2-aminobenzimidazole (400 mg, 3 mmol) and quinoline 2-carboxaldehyde (471 mg, 3mmol) were dissolved in 20 mL of methanol. Approximately 2 drops of acetic acid were added to the solution. Approximately 40 molecular sieves were added, and the solution was refluxed for 48 hours. Once a visible precipitate was formed, the reaction flask was cooled to room temperature. The contents of the reaction flask were added to a beaker and heated, allowing excess methanol to evaporate, resulting in a thick oil. The oil was diluted with dimethyl sulfoxide to 50 mL, resulting in a 60 mM stock solution. Stock was further diluted to 1 mM for fluorescence testing.

Synthesis of L_4. 2-aminobenzimidazole (400 mg, 3 mmol) and quinoline 2-carboxaldehyde (471 mg, 3mmol) were dissolved in 30 mL of methanol. Approximately 3 drops of acetic acid were added to the solution. No molecular sieves were used in this synthesis. The solution was refluxed for 72 hours. Once a visible precipitate was formed, the reaction flask was cooled to room temperature and the precipitate was collected through filtration. The resulting supernatant was then heated to allow for excess methanol to evaporate. Excess ice-cold ultrapure deionized water was added to the supernatant, which allowed for the formation of a precipitate. The precipitate was collected through filtration and washed with ice-cold deionized water to isolate L_4. The resulting supernatant was refrigerated overnight. The supernatant was filtered once more to isolate a third precipitate.

Synthesis of L_5. 2-aminobenzimidazole (400 mg, 3 mmol) and quinoline 2-carboxaldehyde (471 mg, 3mmol) were dissolved in 30 mL of methanol. Approximately 3 drops of acetic acid were added to the solution. Approximately 20 molecular sieves were added, and the solution was refluxed for 24 hours. The reaction flask was cooled to room temperature and was stirred at room temperature for 72 hours. The precipitate was then filtered out and washed with cold methanol.

Synthesis of L_6. Individual solutions of 2-aminobenzimidazole (400 mg, 3 mmol) and quinoline 2-carboxaldehyde (471 mg, 3mmol) in 10 mL ethanol were made. The two solutions were mixed dropwise while stirring. The 20 mL ethanol solution was then refluxed for 4 days. The solution was filtered, isolating a yellow precipitate. The supernatant was then diluted to 50 mL, creating an approximately 30.9 mM stock solution.

Synthesis of L_7. Individual solutions of 2-aminobenzimidazole (400 mg, 3 mmol) and quinoline 2-carboxaldehyde (471 mg, 3mmol) in 10 mL ethanol were made. The two solutions were mixed dropwise while stirring. Approximately 20 molecular sieves were added, and the 20 mL ethanol

solution was then refluxed for 32 hours. The solution was filtered, isolating a yellow precipitate. The supernatant was then heated to evaporate excess ethanol. Excess ice-cold ultrapure deionized water was added to the supernatant, which caused the formation of a precipitate. The precipitate was collected through filtration and washed with ice-cold deionized water to isolate L_7.

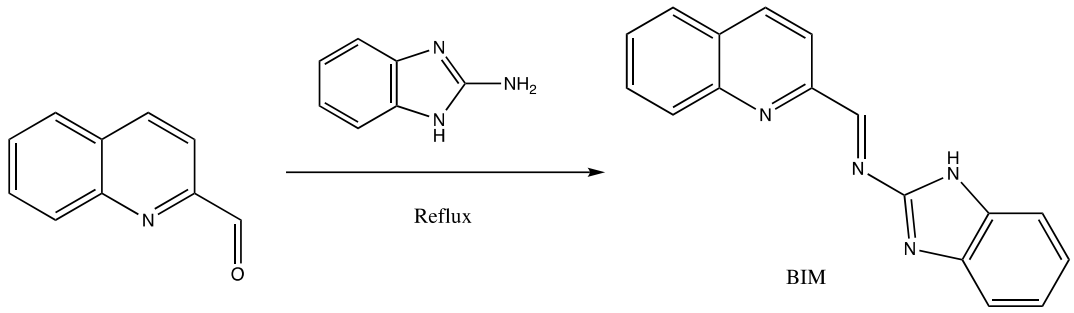

Figure 2.1: Synthesis of BIM

2.4 Preparation of N-[Tris(N-ethyl-1,8-naphthalimide)]amine (NET)

A 2 mL ethanolic solution of Tris(2-aminoethyl)amine (TAEA) (Sigma Aldrich, 96%, 0.1462 g, 1 mmol) was added dropwise to 8 mL of an ethanolic solution of 1,8-naphthalic anhydride (0.6637g, 3.2 mmol,) in a round bottom flask. The mixture was then refluxed for 4 hours, at which point, it was allowed to cool to room temperature. The reaction mixture was then poured into 50 mL of ultrapure deionized water, causing the formation of a precipitate. The precipitate was then filtered, washed with deionized water, and dried to isolate the product as a white solid.

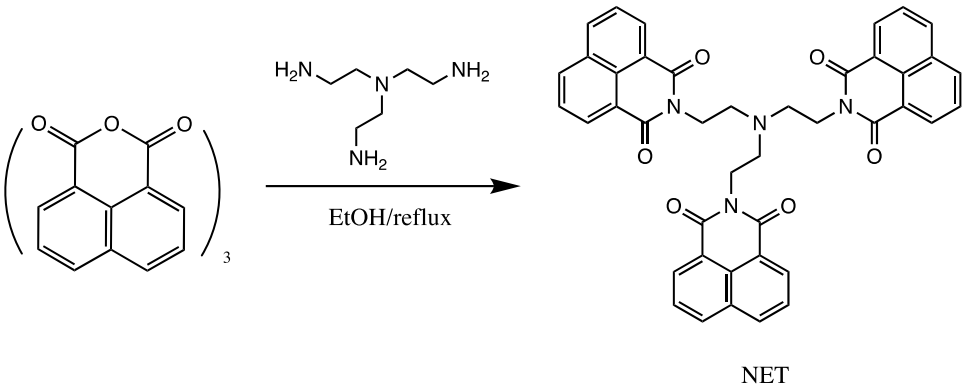

Figure 2.2: Synthesis of NET

2.5 Preparation of 2-(2-((anthracen-9-ylmethyl)amino)ethyl)-3',6'-bis(diethylamino)spiro[isoindoline-1,9'-xanthen]-3-one (AMAE-RhB)

An ethanolic solution of Rhodamine B (Alfa Aesar, 4.79 g, 10 mmol, 30 mL) was added dropwise to a 100 mL glass round bottom flask containing 10 mL of anhydrous ethylenediamine (GFS Chemicals, >99%). The mixture was then refluxed for 20 hours. The solution was allowed to cool to room temperature. The solution was then filtered, washed with cold anhydrous ethanol, and dried, isolating the intermediate compound as a white precipitate.

An ethanolic solution of the intermediate compound (484.3 mg, 1 mmol, 20 mL) was prepared in a 50 mL round bottom flask. 9-anthracenecarboxaldehyde (Sigma Aldrich, >97%, 206.2 mg, 1 mmol) was added to the flask while stirring. The mixture was then refluxed for 7 hours. The solution was allowed to cool to room temperature, at which point sodium borohydride (Sigma Aldrich, ≥98%, 378.3 mg, 10 mmol) was added to the reaction flask while stirring. The mixture was then refluxed again for another 2 hours. The solution was allowed to cool to room temperature. A precipitate was not observed so the reaction flask was refrigerated overnight, where then a precipitate was formed. The mixture was filtered and washed with cold ethanol to isolate a light yellow crystalline solid.

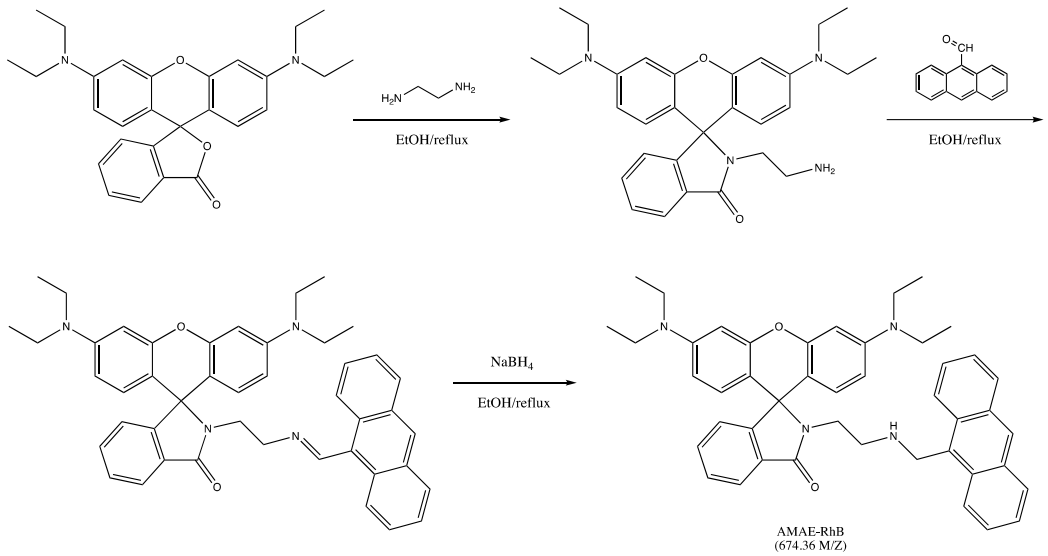

Figure 2.3: Synthesis of AMAE-RhB

2.6 Fluorophore Testing

2.6.1 BIM Fluorescence Testing

Fluorescence samples were prepared using 1 mM dye stock solutions using dimethyl sulfoxide (DMSO) (Fisher Bioreagents, ≥99.7%) as solvent. For the ethanol precipitates, ethanol was used to create the stock solutions in place of DMSO. Samples were prepared in 4 mL borosilicate glass test tubes. An excitation wavelength of 405 nm was used to excite the samples and the emission spectrum was collected from 420-600 nm. For initial fluorescence testing of products, 30 µL of 1 mM stock solution and 30 µL of 2.5 mM aqueous $FeCl_3$ (Sigma Aldrich, ≥99.99%) was added to a test tube and diluted to 3 mL using ultrapure deionized water. For time dependent fluorescence testing, samples were prepared as described previously and the fluorescence was measured after set time intervals.

For further ion testing, stock solutions of various metal salts were prepared at 1 mM using ultrapure deionized water. Concentrated HCl was added to the stock solution of CuCl to fully dissolve the solid salt. Ion samples were prepared at 25 µM for fluorescence testing. Aqueous solutions of

sodium hydroxide and hydrochloric acid were used to adjust the pH of tested samples, including NET and AMAE-RhB samples.

2.6.2 NET Fluorescence and UV-Vis Absorption Testing

Fluorescence samples were prepared using 0.5 mM dye stock solutions using dimethylformamide (DMF)(Sigma Aldrich, ≥99.8%) as solvent. Samples were prepared in 4 mL borosilicate glass test tubes, with a final NET dye concentration of 10 μM. 1 mM ion stock solutions were used to prepare the samples containing metal ions, with a final ion concentration of 100 μM. A DMF/H_2O (2:3; v/v) solvent mixture was used when diluting fluorescence samples. Samples were adjusted to the same pH level. An excitation wavelength of 346 nm was used to excite the samples and the emission spectrum was collected from 450-600 nm.

Samples used for UV-Vis testing were also prepared in a 2:3 DMF/H_2O solvent mixture. Using the 0.5 mM dye stock solution, NET was dissolved in the solvent mixture to a concentration of 10 μM. The 2:3 DMF/H_2O solvent mixture was used as a reference during testing.

2.6.3 AMAE-RhB Fluorescence Testing

Fluorescence samples were prepared using 1 mM dye stock solutions using ethanol as solvent. Samples were prepared in 4 mL polystyrene cuvettes (Sigma Aldrich), with a final dye concentration of 10 μM. 1 mM ion stock solutions were used to prepare samples containing metal ions, with a final ion salt concentration of 10 μM. A 10 mM Tris-HCl buffer in Ethanol/H_2O (1:9; v/v) was prepared at a pH value of 7 and used when diluting fluorescence samples. An excitation wavelength of 560 nm was used to excite the samples and the emission spectrum was collected from 500-700nm.

3 Results

3.1 Literature background on choice of fluorescent dye

One potential method to detect corrosion that we have proposed involves the use of a smart fluid that can chemically detect dissolved Fe^{3+} and Fe^{2+} cations. Pipelines are primarily composed of iron and, through the corrosion process, free Fe^{2+} cations are produced. Fe^{3+} cations are typically not produced due to relatively low O_2 content; however, if there is a leak somewhere in the pipeline, oxidizing agents present in air can cause the formation of Fe^{3+} cations. By detecting both cations separately, spots of local corrosion and possible leaks can be addressed simultaneously.

In this work, our method for detecting Fe^{2+} involves the use of a solution containing fluorescent chemosensors that selectively fluoresce when bound to either Fe^{2+} or Fe^{3+} cations in solution. This fluid would be injected into the gas stream and an optical sensor would be deployed. Fluid injection and optical sensing will be deployed in a cleaning rig referred to as the "PIG" (Pipeline Inspection Gauge). Modern "Pigs" are already typically equipped with integrated sensors and instruments to monitor the pipeline over hundreds of miles during routine cleaning, such as magnetic flux leakage and ultrasonic sensors to monitor for cracks, as well as tilt sensors and odometers to measure distance traveled within the pipeline. Instrumentation needed for our method would be simple to install on currently used pigs.

In addition to the use of position detection sensors, iron cation concentrations can be directly monitored along the gas line utilizing selective fluorescence and specific spots of concern can be located and addressed. Through this method, there would not be any need for concern about hold ups at any of the pipeline features, such as extreme bends and pipeline junctions. Another clear advantage of this method stems from the detection of iron cations. This detection is directly sensitive to corrosion rather than water accumulation or any other variable current methods are set to detect, giving a definite quantification to corrosion levels along the pipeline.

This method of corrosion detection involves the use of two different fluorescent probes, one that fluoresces only in the presence of Fe^{2+} and another that fluoresces only in the presence of Fe^{3+}. The use of dual probes allows for the quantification of both ferric and ferrous ion concentrations independently in the same sample. To accurately measure the concentration of the target cation, the fluorescent chemosensors must exhibit high selectivity towards only the cation of interest. The selected probes must also have a unique emission wavelength range in order to differentiate the emission between the iron cations. The enhancement of emission intensity must also have a range of linear relationship with the concentration of the target metal cation in order to

accurately measure concentrations of both species. Only probes that show an increase in emission intensity in the presence of the target cation, or “turn-on” probes, were considered.

Several studies have reported fluorescent chemosensors that selectively fluoresce in the presence of Fe^{2+} cations. Among them, a compound reported by Hirayama et al. showed the most promise [1]. The compound, named SiRhoNox-1, is a silicon-rhodamine-based dye (structure shown in Fig. 3.1) that shows a significant increase in fluorescence in the presence of Fe^{2+} cations at a maximum emission wavelength of 662 nm when irradiated with 635 nm light (Fig. 3.1(a)). The dye was reported to be extremely selective, showing no fluorescence enhancement in the presence of multiple other metal cations (Fig. 3.1(b)). Samples were tested in 50 nM HEPES buffer at pH 7.4. There is a reported time delay before samples containing Fe^{2+} give a maximum fluorescence intensity (Fig. 3.1(c)). The fluorescence intensity begins to plateau after about 2000 seconds from sample creation at room temperature. This compound is available commercially under the name FerroFarRed from Goryo Chemicals. Samples were purchased and tested, confirming the results reported in the literature.

Once a promising candidate for the ferrous iron probe was found, attention was directed towards finding a suitable probe for ferric cations. In this work, three different fluorescent tag compounds were synthesized, characterized, and tested for their fluorescence properties. These compounds are as follows:

1. (E)-N-(1H-benzo[d]imidazol-2-yl)-1-(quinolin-2-yl)methanimine (BIM)
2. N-[Tris(N-ethyl-1,8-naphthalimide)]amine (NET)
3. 2-(2-((anthracen-9-ylmethyl)amino)ethyl)-3',6'-bis(diethylamino)spiro[isoindoline-1,9'-xanthen]-3-one (AMAE-RhB)

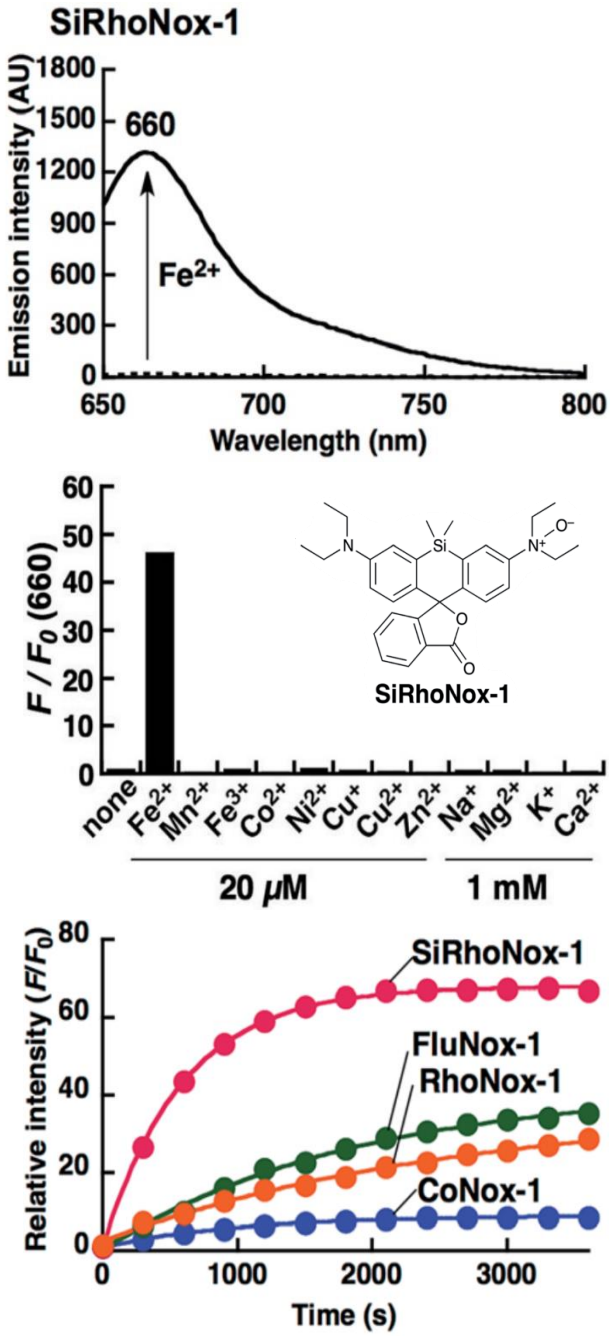

Figure 3.1: Reported data of SiRhoNox-1 Fe^{2+} fluorescent tag. (a) Fluorescence spectra of SiRhoNox-1 (2 μM) upon addition of $FeSO_4$ (20 μM) in 50 mM HEPES buffer (pH 7.4) (λ_{ex} = 630 nm). (b) Emission intensity of SiRhoNox-1 against several metal cations measured 1 hour after sample creation. (λ_{em} = 660 nm). Inset shows the structure of SiRhoNox-1. (c) Time measurements of the relative fluorescence intensity of SiRhoNox-1 (red) in the presence of $FeSO_4$ (λ_{em} = 660 nm) [1].

Kar et al. reported a novel quinoline functionalized Schiff base (BIM) that showed high fluorescence sensitivity towards Fe^{3+} cations [2]. The reported procedure to synthesize the BIM dye involved a simple one-step reflux reaction. In the presence of one equivalent of ferric cations, the dye is reported to have a large peak centered at 500 nm when irradiated with 405 nm light (Fig. 3.2). This excitation and emission wavelength is compatible with our candidate for the ferrous iron probe. The dye shows high selectivity for Fe^{3+}; however, it also gives increased fluorescence intensity in the presence of Al^{3+} and Cr^{3+}.

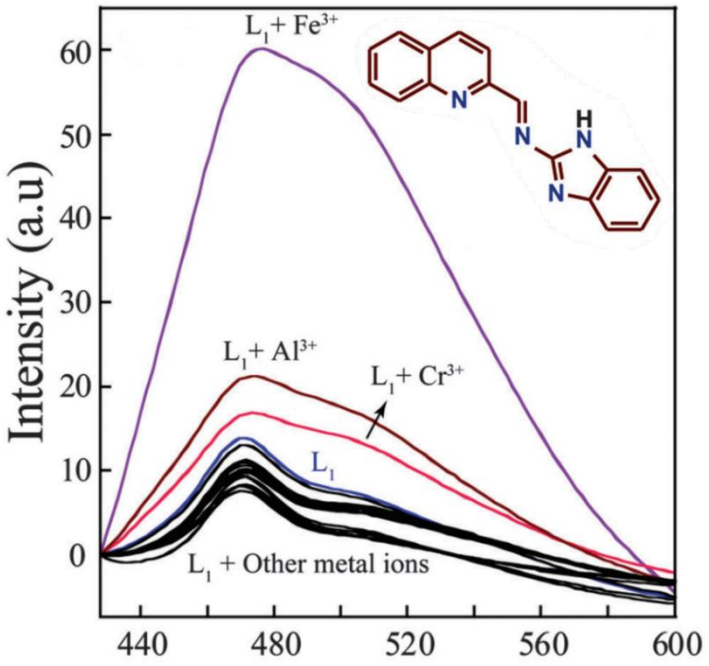

Figure 3.2: Reported fluorescence spectra of BIM (10 µM) in the presence of Fe^{3+} and other metal ions (20 µM) in 1 mM 1:4 CH_3CN/aqueous HEPES buffer at pH 7.3 (λ_{ex} = 405 nm). Inset shows the structure of BIM. [2]

Another fluorescent chemosensor of interest that could possibly be used as a ferric cation probe was reported by Yang et al. [3]. They synthesized a 1,8-naphthalimide based ligand (NET) that was also reported to have a high fluorescence selectivity towards Fe^{3+}. Previously, 1,8-naphthalimide-based derivatives have shown promise as fluorescent chemosensors for selectively detecting different metal cations in solution [4-6]. The synthetic procedure for NET also involved a one-step reflux reaction. With an excitation wavelength of 346 nm, NET produced a maximum emission intensity at 495 nm in the presence of Fe^{3+} cations (Fig. 3.3(a)), which is compatible with the SiRhoNox-1 dye. This increase in fluorescence intensity was not reported with other cations and is sustained at pH levels under pH 6.4 (Fig. 3.3(b)). At pH 3.1, NET begins to fluoresce without the presence of Fe^{3+}, giving NET a pH range of 3.1-6.4 where it is usable as a fluorescent probe for Fe^{3+}.

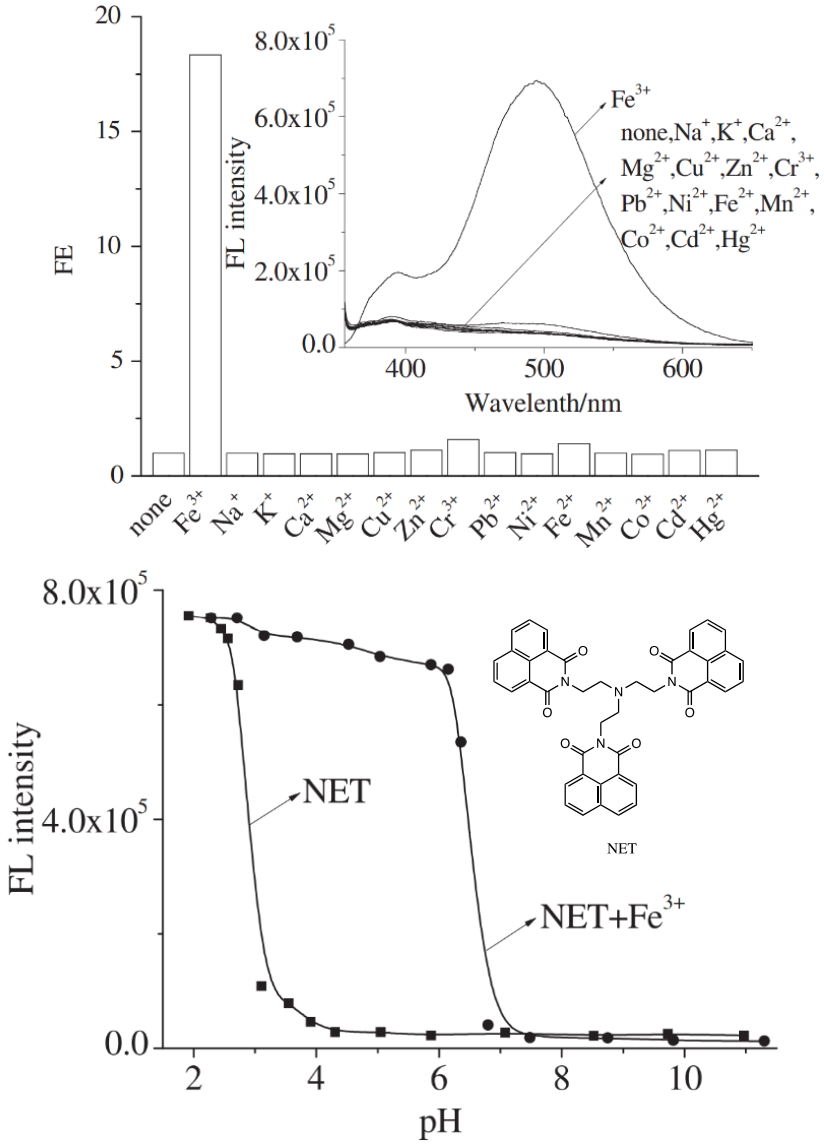

Figure 3.3: Reported data of the NET Fe^{3+} fluorescent tag. (a) Emission intensity of NET (10 µM) against several metal cations (100 mM) in 2:3 DMF/H_2O (λ_{em} = 495 nm, λ_{ex} = 346 nm). Inset shows the full fluorescence spectrums for each ion sample. (b) Fluorescence emission intensity of NET (squares) and NET + Fe^{3+} (circles) at different pH levels (λ_{ex} = 340 nm). Inset shows the structure of NET. [3]

A third potential ferric iron probe was also considered. Rhodamine B derivatives have previously shown the ability to selectively fluoresce in the presence of metal cations [8]. This increase in fluorescence is believed to occur due to an opening of the spirolactam ring after binding to the metal cation. This selectivity can be tuned to different metal ions by changing the nitrogen-bound substituent group attached to the spirolactam group [9-11]. Jin et al. reported a Rhodamine B-based compound (AMAE-RhB) that gave a fluorescence emission maximum at 582 nm in the presence of ferric cations using an excitation wavelength of 560 nm (Fig. 3.4(a)). The reported procedure to synthesize the compound was slightly more complicated than the previous two dyes, involving two reflux steps and a reduction using sodium borohydride. Comparing AMAE-RhB to the NET and BIM dyes in the presence of ferric iron, the emission wavelength range shifts closer to the wavelength range emitted by FerroFarRed with Fe^{2+}, however, the wavelength ranges do not overlap with either emission maxima, allowing for AMAE-RhB to be another viable candidate for an Fe^{3+} probe. Hg^{2+} also gives a substantial increase in fluorescence intensity. This would not be an issue in our proposed application as mercury is typically removed before transportation. Fig. 3.4(b) shows the reported pH dependance of AMAE-RhB's fluorescence. The dye without any added cations shows no intensity over the reported range of pH 2-12. In the presence of Fe^{3+}, AMAE-RhB fluoresces at pH $\leq$ 8 of the range reported, giving a maximum intensity at pH 5-7. From this data, AMAE-RhB has the potential to be used as a fluorescent tag for Fe^{3+} for pH $\leq$ 8.

In this study, these three selected fluorescent tags were synthesized and characterized for their fluorescent properties in order to confirm the reported data. Experimental methods, including synthetic procedures, instrumentation, and instrumentation methods, are reported in the Experimental section. Collected data and fluorescence spectra, discussion of the observed trends, including the observed pH dependance of each tag's fluorescence are described in the following sections.

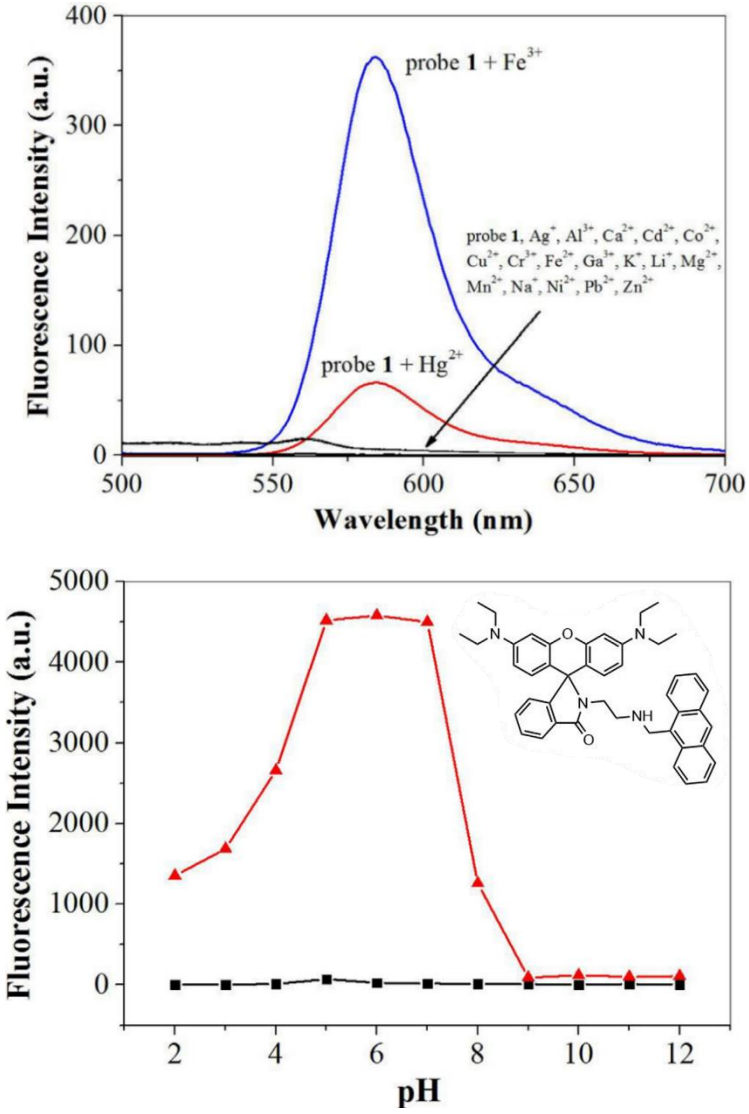

Figure 3.4: Reported data of the AMAE-RhB Fe^{3+} fluorescent tag. (a) Fluorescence spectra of AMAE-RhB (5 µM) in the presence of Fe^{3+} and other metal ions (5 µM) in Tris-HCl buffer (1:9 EtOH/H_2O, pH 7.0) (λ_{ex} = 560 nm). (b) Fluorescence emission intensity of AMAE-RhB (squares) and AMAE-RhB + Fe^{3+} (triangles) at different pH levels (λ_{em} = 582 nm, λ_{ex} = 560 nm). Inset shows the structure of AMAE-RhB [7].

3.2 SiRhoNox-1 (FerroFarRed) as fluorescent dye for Fe^{2+}

Selective binding of a florescent tag, FerroFar Red (SiRhoNox-1) to Fe^{2+} in an aqueous solution is demonstrated in this work. To perform this work, we had purchased several fluorescent dyes including FerroFarRed and several salts including simple salts of Fe^{2+}, Fe^{3+}, Ni^{2+}, Cr^{3+}, Cu^{+}, Al^{3+}, Ca^{2+}, Na^{+}, K^{+}, Mg^{2+}, Mn^{2+}, Co^{2+}, Zn^{2+}. Figure 1 shows the structure and of the fluorescent tag FerroFarRed that has an excitation wavelength of 630 nm and detected at 660 nm and the experimental schematic for chelating the tag to the metal center. The concentration of the metal ions and tag were kept in the µM regime. Figure 3.5 shows selective binding of the fluorescent tag to Fe^{2+}.

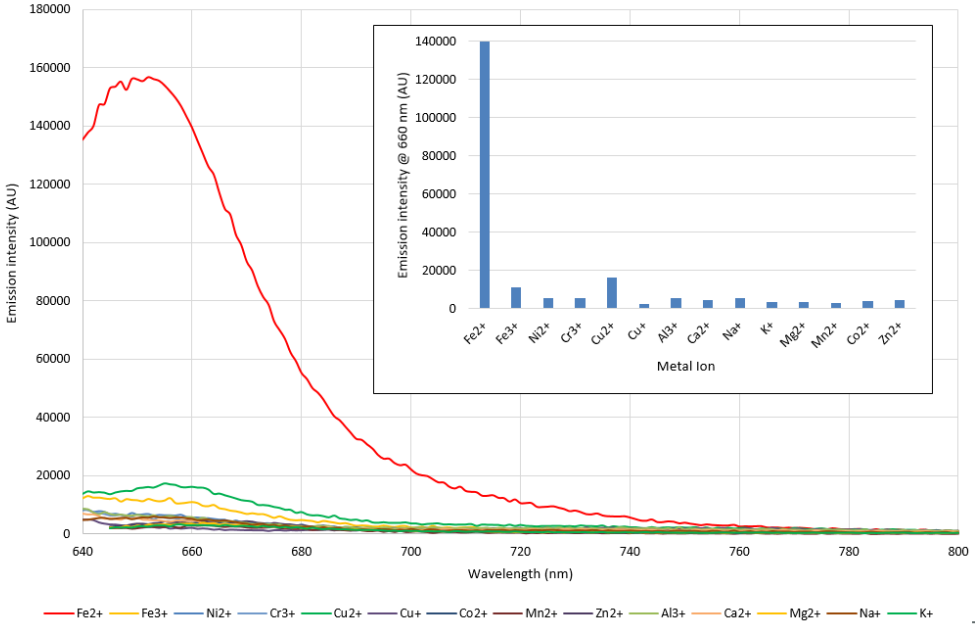

Figure 3.5: Fluorescence of FerroFarRed (SiRhoNox-1)-metal ion complex excited at 630 nm and detected at 660 nm. Initial metal cation ion concentration is around 20 uM and 1uM for alkali and alkali earth cations and the tag concentration was 2 uM.

FerroFarRed requires an incubation time of 1 hr at 37 ^{o}C to complex with the metal ions, as described in the literature. We had therefore explored the effect of time and temperature on the fluorescence dependence of Fe^{2+} as shown in Figure 3.6. We found that the fluorescence signal is attenuated at room temperature. The fluorescence signal increases with complexation time between 0 to 45 min. Interestingly, the complex remains stable, such that even after 3 days of complexation, a significant amount of fluorescence signal can still be detected.

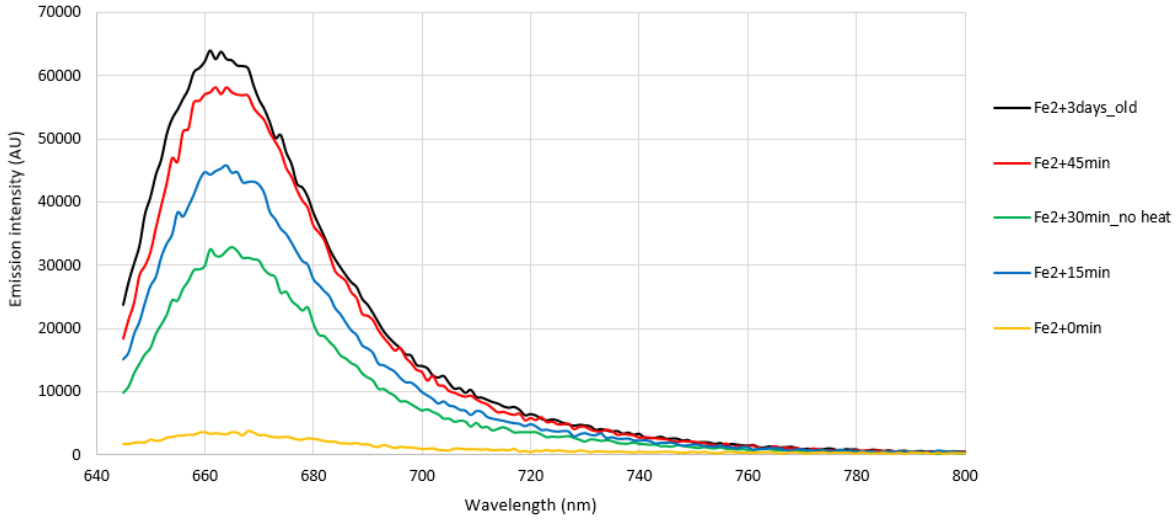

Figure 3.6: Fluorescence of FerroFarRed (SiRhoNox-1)-metal ion complex excited at 630 nm and detected at 660 nm as a function of time and temperature. Initial metal cation ion concentration is around 20 uM and 1uM for alkali and alkali earth cations and the tag concentration was 2 uM.

Building upon the success of the fluorescent tag that selectively binds to Fe^{2+} in the presence of several metal salts, we have turned our efforts on identifying and synthesizing a different fluorescent tag for the selective detection of Fe^{3+} such that various tags can be introduced to the fluid to detect the presence and determine the speciation of the Fe species. We have conducted a literature search and identified fluorescent tag candidates for complexing with Fe^{3+}. These compounds are:

1. (E)-N-(1H-benzo[d]imidazol-2-yl)-1-(quinolin-2-yl)methanimine (BIM)
2. N-[Tris(N-ethyl-1,8-naphthalimide)]amine (NET)
3. 2-(2-((anthracen-9-ylmethyl)amino)ethyl)-3',6'-bis(diethylamino)spiro[isoindoline-1,9'-xanthen]-3-one (AMAE-RhB)

3.3 BIM Dye

3.3.1 Synthesis and Initial Fluorescence Testing of BIM Dye

The procedure to synthesize (E)-N-(1H-benzo[d]imidazol-2-yl)-1-(quinolin-2-yl)methanimine (BIM) outlined in the original literature was followed but did not yield the solid yellow precipitate that was described. Different synthetic routes were attempted to create and isolate the target compound. By extending the reflux time to 20 hours a solid bright yellow precipitate was isolated, however it did not fluoresce as described in the literature. In the presence of Fe^{3+}, samples prepared with this precipitate did not show any increase in fluorescence intensity over samples prepared without iron. By adding cold water to the supernatant, a precipitate (L_2) was isolated that gave similar fluorescence to the dye reported in the literature. The synthesis was repeated with a longer reflux time of 48 hours in order to increase yield. The initial precipitate showed no fluorescence enhancement with Fe^{3+} while Figure 3.7 shows the fluorescence spectra of the precipitate isolated using cold water. Samples prepared without metal ions showed no significant intensity. When Fe^{2+} is added, there was no observable change in the collected spectrum. Upon addition of Fe^{3+}, a broad large peak is seen centered at 500 nm, matching the fluorescence data for BIM reported in the literature. A large sharp intensity centered at 471 nm can be attributed to the presence of water.

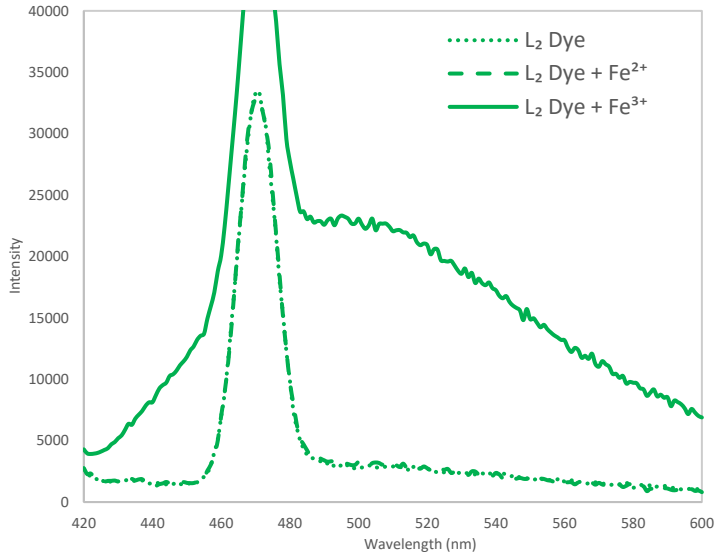

Figure 3.7: Fluorescence spectrums of the L_2 precipitate (10 µM) and the precipitate with $Fe(NH_4)_2(SO_4)_2$ (10 µM), and with $FeCl_3$ (25 µM). (λ_{ex} = 405 nm)

While the fluorescence enhancement of the L_2 precipitate occurred at the reported emission wavelength, the observed intensity was low, indicating possible impurities. Other synthetic procedures were attempted in order to produce a more pure and viable dye. Figure 3.8 shows the fluorescence emission at 500 nm of several dyes that were synthesized. The L_4 precipitate showed the most promise of all the synthetic procedures attempted, with the greatest increase in intensity with iron for all the products tested. The yield of that precipitate, however, was considerably low (approx. 30 mg).

Another study that synthesized the same ligand was found. The procedure reported in that study was similar to the original synthetic process used to synthesize the L_2 precipitate, however there were minor differences, such as the use of ethanol as solvent instead of methanol used in the previous synthesis. This synthesis also required the addition of cold water to precipitate out a product (L_7) that gave an observable fluorescence enhancement with iron. The fluorescence spectra for this dye are displayed in Figure. 3.9. The shape and position of the enhancement remains the same as the previous L_2 precipitate, with an increased intensity for the peak at 500 nm.

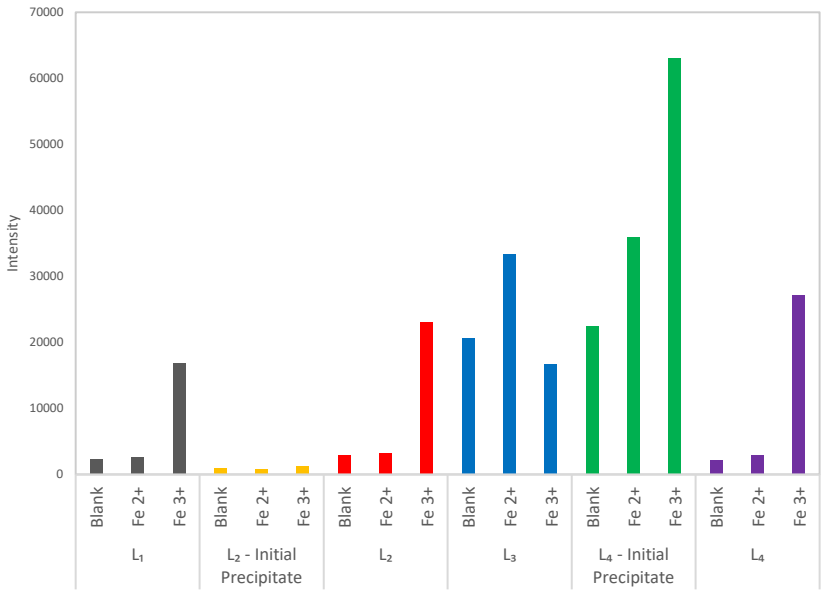

Figure 3.8: Fluorescence emission at 500 nm of several different synthetic procedures. Samples contained dye (10 µM) , dye (10 µM) with $Fe(NH_4)_2(SO_4)_2$ (10 µM), and dye (10 µM) with $FeCl_3$ (25 µM) (λ_{ex} = 405 nm)

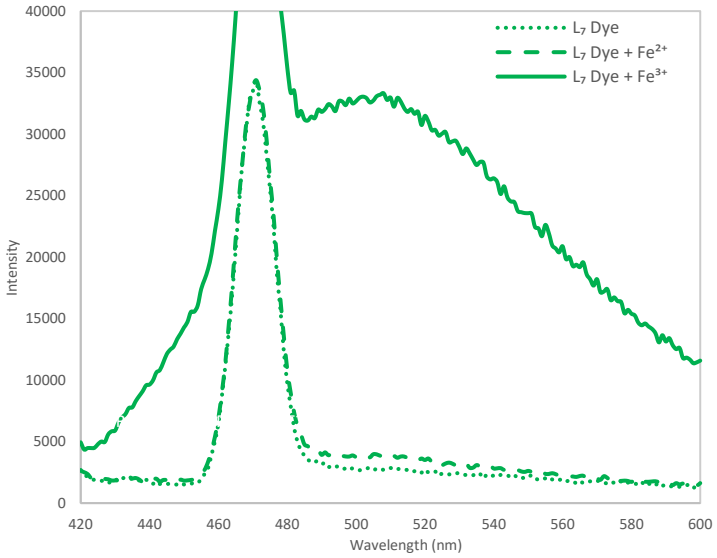

Figure 3.9: Fluorescence spectrums of the L_7 precipitate (10 µM) and the precipitate with $Fe(NH_4)_2(SO_4)_2$ (10 µM), and with $FeCl_3$ (25 µM). (λ_{ex} = 405 nm)

3.3.2 Characterization of BIM Precipitate

The spectrum of this precipitate still showed a lower emission intensity compared to literature, so TLC analysis was performed on the products precipitated using water. Fig. 3.10 shows the chromatography plates for these tests. Evidence of a newly formed species was observed as separate new green spots on the TLC plate using a UV lamp with a wavelength of 365 nm. Spots were also observed at the same locations for both RM2 (quinoline-2-carboxaldehyde) and for each precipitate. This may indicate the presence of starting material in the synthesized product. These spots could also originate due to reactivity with the mobile phase. Multiple spots are seen for quinoline carboxaldehyde when only one is expected. This irregularity may originate from the analyte breaking down in the solvent mixture.

In order to quantify the potential impurities, samples were created with increasing dye concentration and a fixed Fe^{3+} concentration. The fluorescence emission at 500 nm for each dye concentration is displayed in Fig. 3.5. This precipitate showed a maximum in emission intensity at a dye concentration of about 40-50 µM with 25 µM Fe^{3+}. The maximum emission from this

precipitate approaches the intensity observed from the original 20-hour dye. As shown in the original study, the ideal ratio of dye and Fe^{3+} is 1:1.

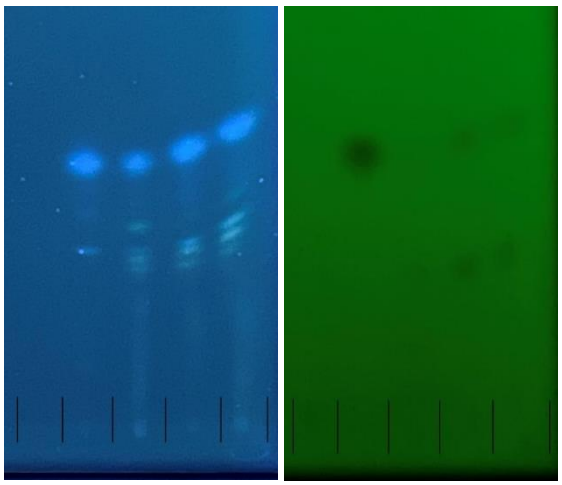

Figure 3.10: TLC Plates of starting materials and precipitates using ethyl acetate, methanol, and hexanes (1:1:8) as mobile phase. RM1 and RM2 are 2-aminobenzimidazole and quinoline-2-carboxaldehyde. PPT1, PPT2, and PPT3 are three L_7 precipitates synthesized using the same method.

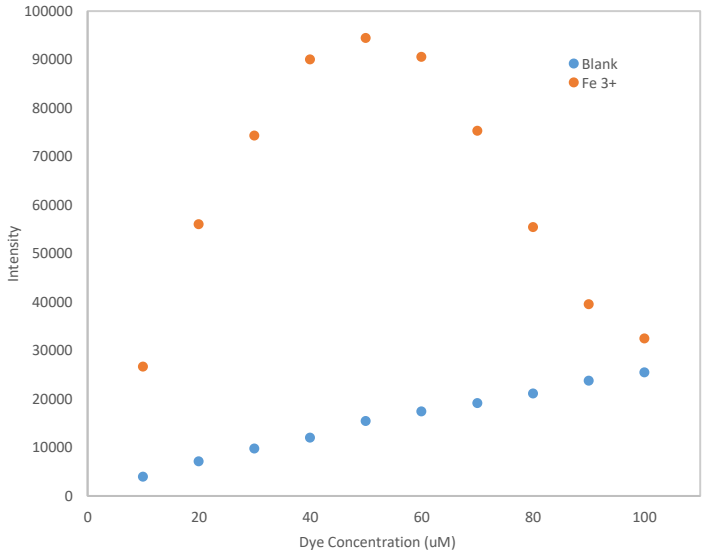

Figure 3.11: Fluorescence emission intensity (505 nm) of increasing L_7 dye concentration with fixed $FeCl_3$ (25 μM). (λ_{ex} = 405 nm)

To probe whether starting materials are present in the final product, ESI mass spectrometry was performed on the dye. This spectrum is shown in Fig. 3.12. Small peaks are seen at 134.07 (14.3%) and 158.06 m/z (2.1%), which corresponds to 2-aminobenzimidazole and quinoline-2-carboxaldehyde respectively. This result reduces the likelihood that the TLC spots seen previously originated from the presence of starting material. The molecular ion peak is seen at 273.11 m/z, which correlates to a protonated BIM molecule. The inset shows an expanded view of the molecular ion peak. Individual peaks are seen at 273.11 (100%), 274.12 (19.45%), and 275.12 m/z (1.81%). This matches the expected isotopic pattern for the BIM molecule. Peaks are also seen at 319.16 (86.7%), 637.3 (32.3%), and 955.4 m/z (2.5%). The peak at 319.16 m/z corresponds to a BIM molecule with an attached ethanol molecule and a bound proton. The ethanol may originate from the synthesis, as ethanol was used as the solvent during the reflux step. Ethanol was also used to dissolve the precipitate for mass spectrometry, which may be another potential source for this peak. The peaks at 637.2 and 955.4 m/z correlate with the mass of a dimer and trimer of the BIM molecule with the attached ethanol. Reducing the concentration of precipitate causes these two peaks to disappear, indicating that they originate from dimers and trimers.

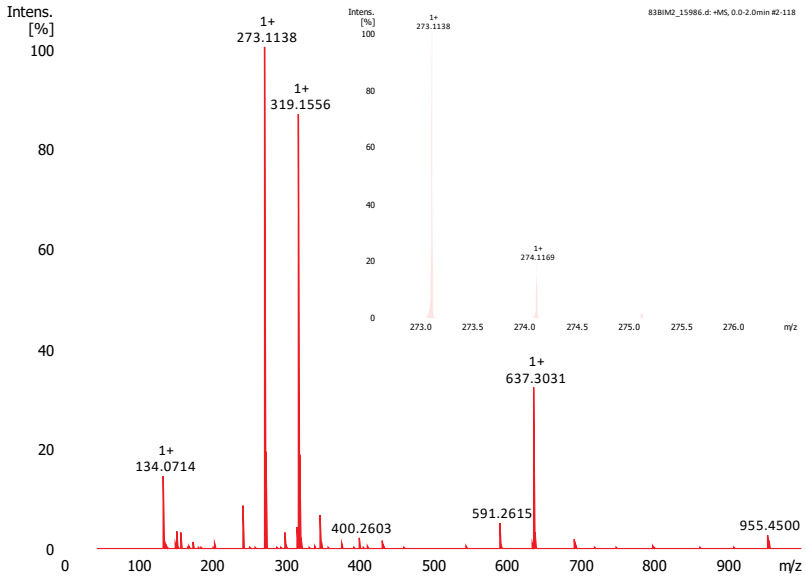

Figure 3.12: ESI Mass Spectrum of L_7 Dye. Inset shows an expanded view of the molecular ion

^{1}H NMR was also performed on the L_7 precipitate. Fig. 3.13 shows the collected spectrum while the inset shows an expanded view of the 7.5-8.8 ppm range. The peaks observed in this range, in addition to peaks observed at 9.50 and 6.05 ppm, can be attributed to the aromatic protons from the BIM molecule and closely match the NMR data reported in the literature. These results further serve as evidence that the synthesized solid precipitate contained the target BIM molecule. A quintet seen at 2.5 ppm can be attributed to the residual solvent peak from DMSO and a singlet at 3.3 ppm can be attributed to water, occurring due to DMSO's high miscibility with water. In addition to these peaks, several other intensities can be seen in the collected spectrum. These peaks indicate the presence on impurities in the solid precipitate, affirming our suspicions from the initial fluorescence testing.

3.3.3 Effect of Time on BIM Fluorescence

During testing, there was a noticeable decrease in emission over time. Fig. 3.14 shows the emission intensity of the L_7 precipitate/$FeCl_3$ sample after set amounts of time elapsed after sample creation. The sample in this figure was prepared in a 4 mL borosilicate glass test tube. Samples

prepared in other glassware showed an even greater drop in emission intensity. The intensity degradation of the samples may be due to complexation between the borosilicate glass and the Fe^{3+} ions.

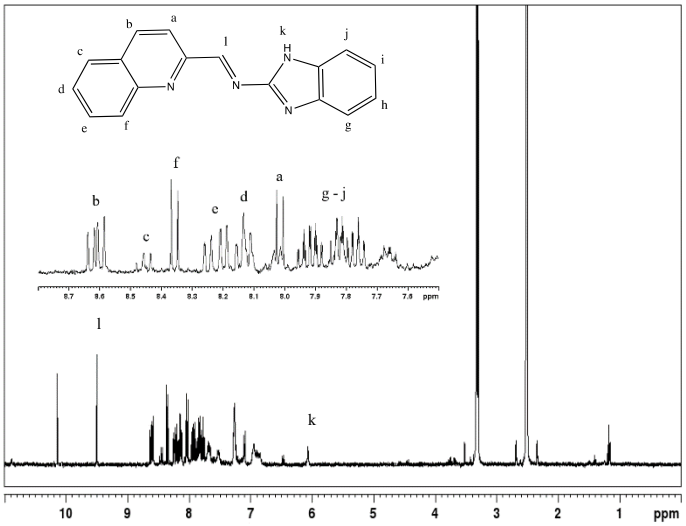

Figure 3.13: ^{1}H NMR spectrum of L_7 Dye in DMSO-D_6.

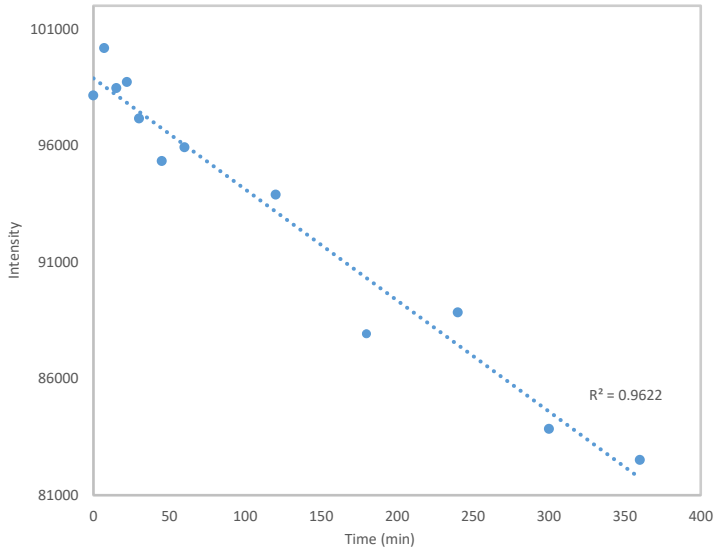

Figure 3.14: Fluorescence emission intensities (505 nm) of the of L_7 precipitate (40 μM) with $FeCl_3$ (25 μM) after various amounts of time had elapsed after sample creation. (λ_{ex} = 405 nm)

3.3.4 Metal Ion and pH Effects on BIM Fluorescence

To quantify the effects of other ions on the dye's fluorescence emission, samples of the dye were prepared with various salt solutions. The salt solutions that produce free Fe^{3+} ions ($FeCl_3$, $FeNO_3$) show the highest intensity, except for the CuCl sample. Strong acid (HCl) was needed to dissolve solid CuCl to make the stock solution. This caused the sample containing CuCl to be considerably more acidic than the other ion samples tested. Samples containing Cr^{3+} and Al^{3+} gave a noticeable fluorescence enhancement as well, which is consistent with the data presented in the original literature. The pH of each ion sample was tested and was also plotted along with the intensity at 505 nm in Fig. 3.15. A noticeable trend emerged where more acidic ion samples had higher emission intensities. This suggested that the intensity of this dye's emission may be pH-dependent, rather than ion-dependent. To test this, four different ion samples were pH adjusted to match the pH of an $FeCl_3$ sample. The emission intensity of these samples at 505 nm is displayed in Fig. 3.16. The intensity of the pH adjusted samples were significantly close to the intensity of the $FeCl_3$ sample, further indicating that the observed fluorescence enhancement is due to pH dependance.

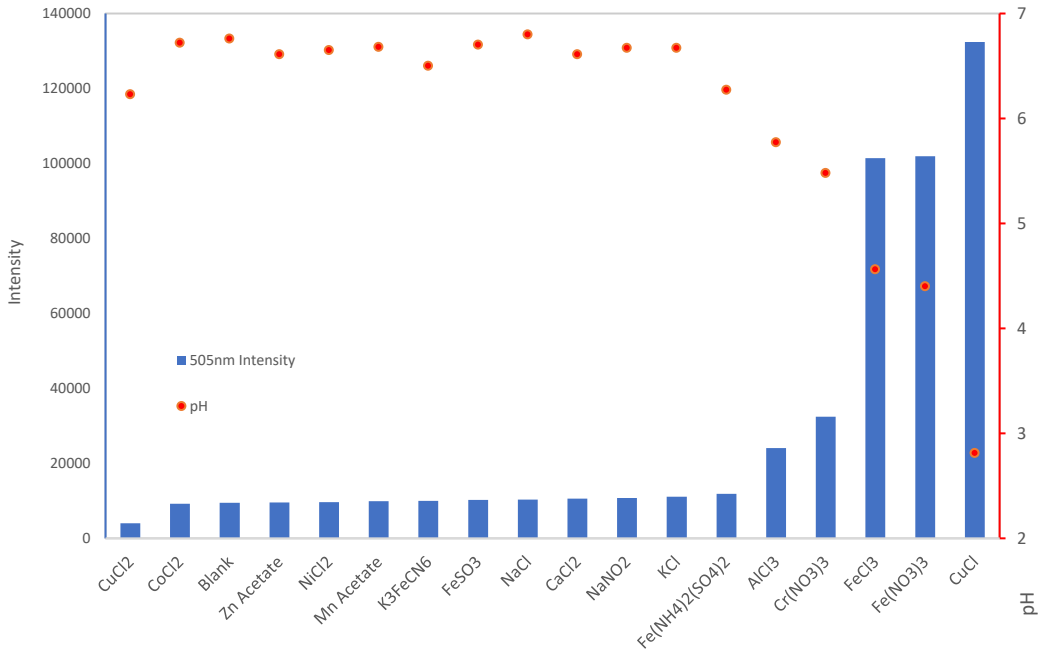

Figure 3.15: Emission intensity (505 nm) and pH of various ion samples (40 µM dye, 25 µM listed salt). (λ_{ex} = 405 nm)

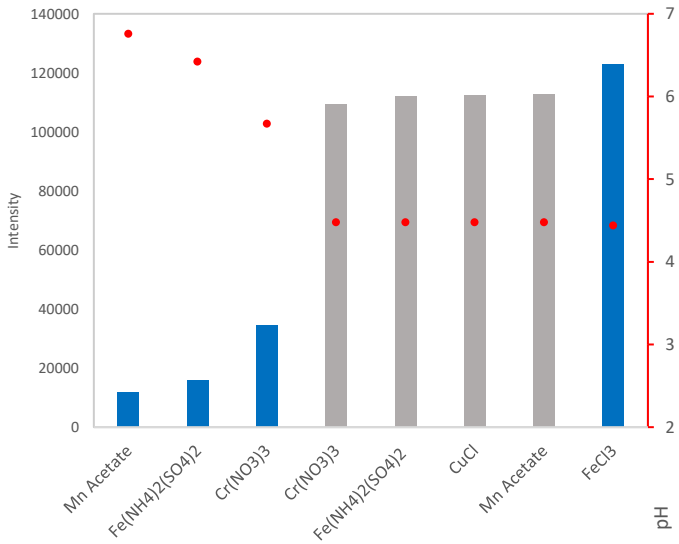

Figure 3.16: Emission intensity (505 nm) and pH of non-pH-adjusted ion samples (blue bar) (40 µM dye, 25 µM listed salt) and pH-adjusted ion samples (gray bar) (40 µM dye, 25 µM listed salt) (λ_{ex} = 405 nm)

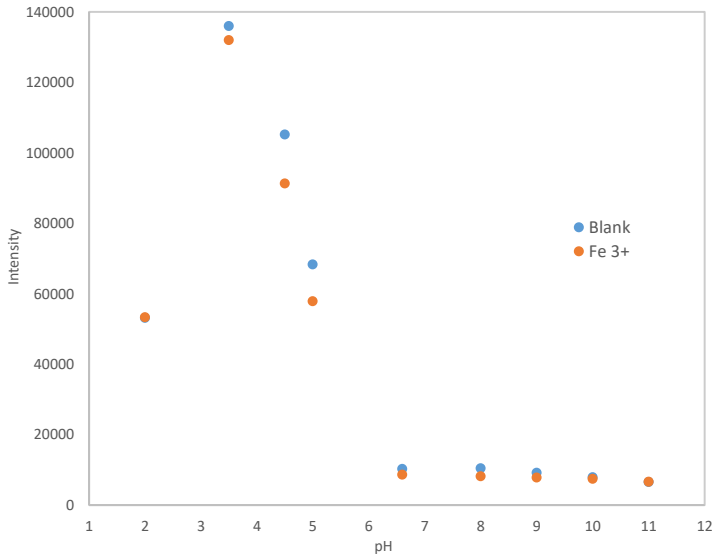

Figure 3.17: Fluorescence emission at 505 nm of L_7 dye (40 µM) with and without Fe^{3+} (25 µM) samples at different pH. (λ_{ex} = 405 nm)

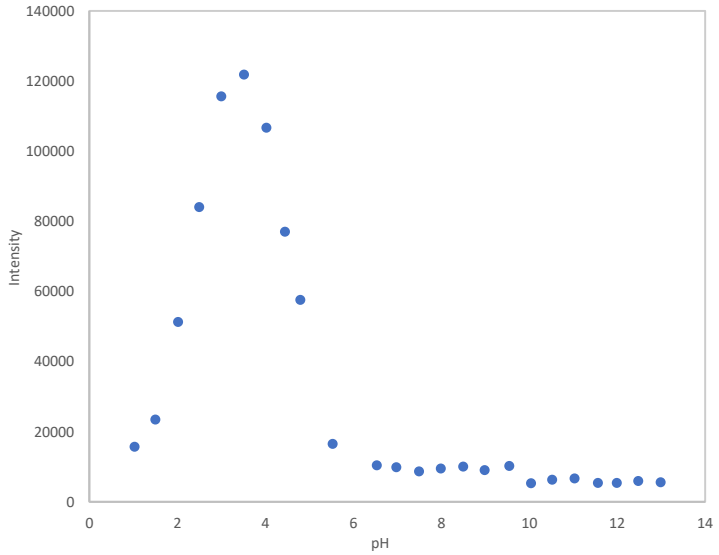

Figure 3.18: Fluorescence emission at 505 nm of L_7 dye (40 µM) at different pH. (λ_{ex} = 405 nm)

To test the pH dependance of this dye, samples of the dye with and without $FeCl_3$ were created and they were pH adjusted to match at various pH values. Fig. 3.17 shows the emission intensity of these samples at 505 nm. For each pH value, the blank dye sample intensity was equal to, or greater than the sample containing Fe^{3+}. The difference in intensity between samples with and without iron is likely due to the intensity time dependance of the ferric samples in glassware discussed previously. The fluorescence intensity of the BIM dye for an expanded pH range is shown in Fig. 3.18. A peak in emission intensity is seen at pH 3.5. The observed trend in intensity for each pH is consistent with the data from previous tests. These results show that the fluorescence of the synthesized product is dependent solely on pH rather than the presence of the tested ions.

3.4 NET Dye

3.4.1 Synthesis and Characterization of NET

N-[Tris(N-ethyl-1,8-naphthalimide)]amine (NET) was synthesized according to the procedure outlined in the literature [3] and described in detail in the experimental section in Chapter 2.2. To confirm the synthesis, Fourier-transform infrared absorption (FTIR) and ^1H NMR spectrums of the synthesized NET were collected and are displayed in Fig. 3.19 and Fig. 3.20 respectively. The FTIR spectrum of NET in Fig. 3.19 shows peaks at 3060 cm^{-1}, 2980 cm^{-1}, and 2850 cm^{-1}. The 3060 cm^{-1} peak corresponds to an aromatic C-H stretch from the 1,8-naphthalimide groups while the 2980 cm^{-1} and 2850 cm^{-1} peaks correspond to alkane C-H stretches from the connecting carbon chain. These peaks match closely with the three peaks at 3064 cm^{-1}, 2969 cm^{-1}, and 2856 cm^{-1} reported in the literature. We consider the small difference in peak position to be minor. The peaks in the fingerprint region (<1500 cm^{-1}) of the FTIR data also match the literature spectrum.

^1H NMR was collected on the synthesized NET. The NMR spectrum in Fig. 3.20 shows peaks at 8.14, 7.83, 7.51, 4.26, and 3.04 ppm, which match the chemical shifts from the literature. Fig. 3.20 also shows which protons these peaks are attributed to. There is little evidence of any impurities in the NMR spectrum. In general, IR and NMR characterization data of the synthesized NET is in close agreement with the literature and suggests the product is relatively pure.

The UV-Vis absorption spectrum of NET is displayed in Fig. 3.21. The absorption of NET is strongly affected by the identity of the solvent. The solvent used to collect this spectrum is a 2:3 DMF/H_2O mixture. An absorption peak range is observed at 325-375 nm, which originates from

the absorption of the 1,8-naphthalimide groups in the molecule. This pronounced peak range is also observed in UV-Vis spectrum of NET in DMF shown in the literature, with both spectrums showing a close similarity. This result further confirms the identity of the synthesized ligand.

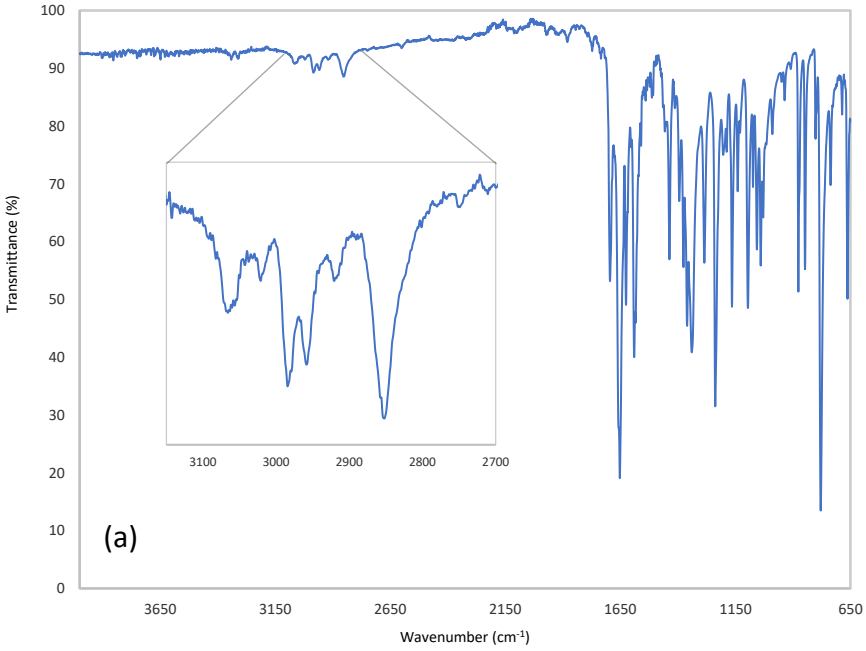

Figure 3.19: ATR-FTIR spectrum of NET. Inset shows an expanded view of 2700-3150 cm^{-1}.

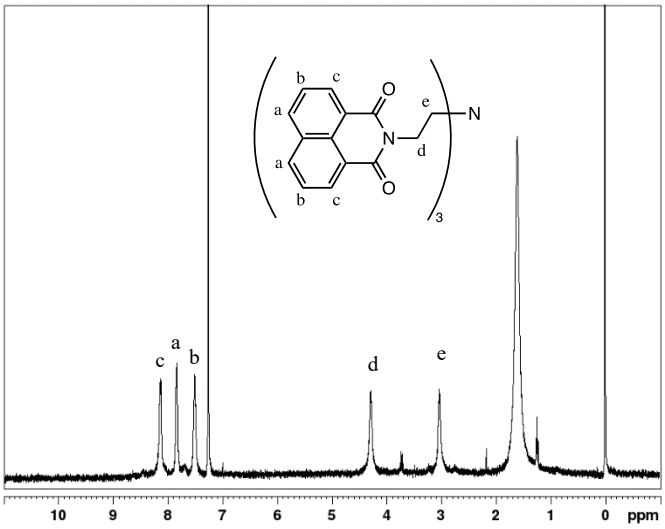

Figure 3.20: ^{1}H NMR of NET in $CDCl_3$ (400 MHz)

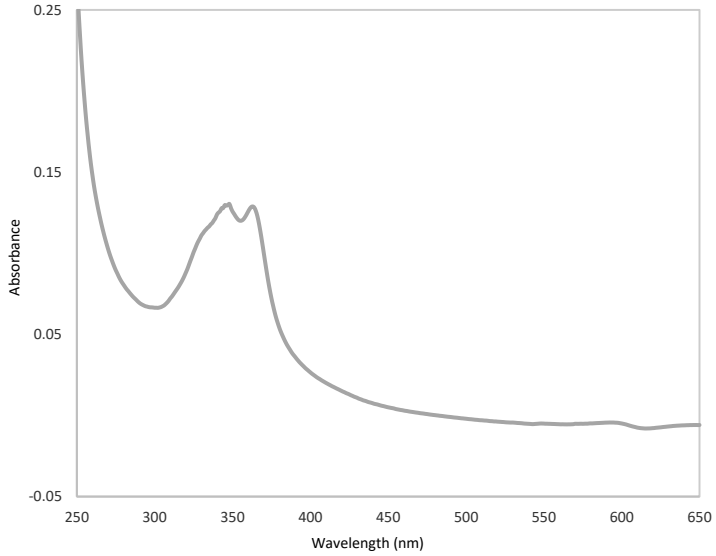

Figure 3.21 UV-Vis Absorption spectrum of NET (10 μM) in 2:3 DMF/H_2O

3.4.2 Metal-Ion NET Complexation Based on Emission Measurements

The fluorescence emission of NET in 4:1 DMF/H_2O and 2:3 DMF/H_2O are shown in Figs. 3.22 (a) and (b) respectively. For both solvent mixtures, NET shows broad flat emission from 370-600 nm. Fluorescence emission peaks from the solvents are observed at 390 nm and 370 nm for the 2:3 DMF/H_2O and 4:1 DMF/H_2O mixtures, respectively. Upon addition of 100 μM $FeCl_3$ in 2:3 DMF/H_2O, additional fluorescence was observed at 495 nm (Fig. 3.22 (b)). In the same spectrum, a smaller secondary peak is also seen at 395 nm. Comparing Fig. 3.22 (a) to (b), the primary emission peak at 495 nm shifts to 490 nm and has a lower intensity. In Fig. 3.22 (a), the secondary peak stays at 395 nm, however, intensity increases significantly, overtaking the intensity of the peak at 490 nm. To ensure the increased intensity was an effect of the Fe^{3+} cation, a sample was made using $Fe(NO_3)_3$. As shown in Fig. 3.22 (b), there is negligible difference between the $FeCl_3$ and $FeNO_3$ precursors, indicating that the increased intensity comes from the presence of the Fe^{3+} cation and not an effect of the anion identity. The spectrum collected using 2:3 DMF/H_2O as solvent is comparable to the spectrum shown in the literature. Both spectra have intensity maxima at 495 nm with smaller secondary peaks at 395 nm. For the samples prepared in 4:1 DMF/H_2O, there was a small peak shift to 493 nm with a slightly reduced intensity compared to the samples prepared in 2:3 DMF/H_2O, similar to what is observed in Fig. 3.22. However, the large peak observed at 393 nm in Fig. 3.22 (a) does not appear in the literature. Due to this discrepancy, 2:3 DMF/H_2O was used as solvent for further tests.

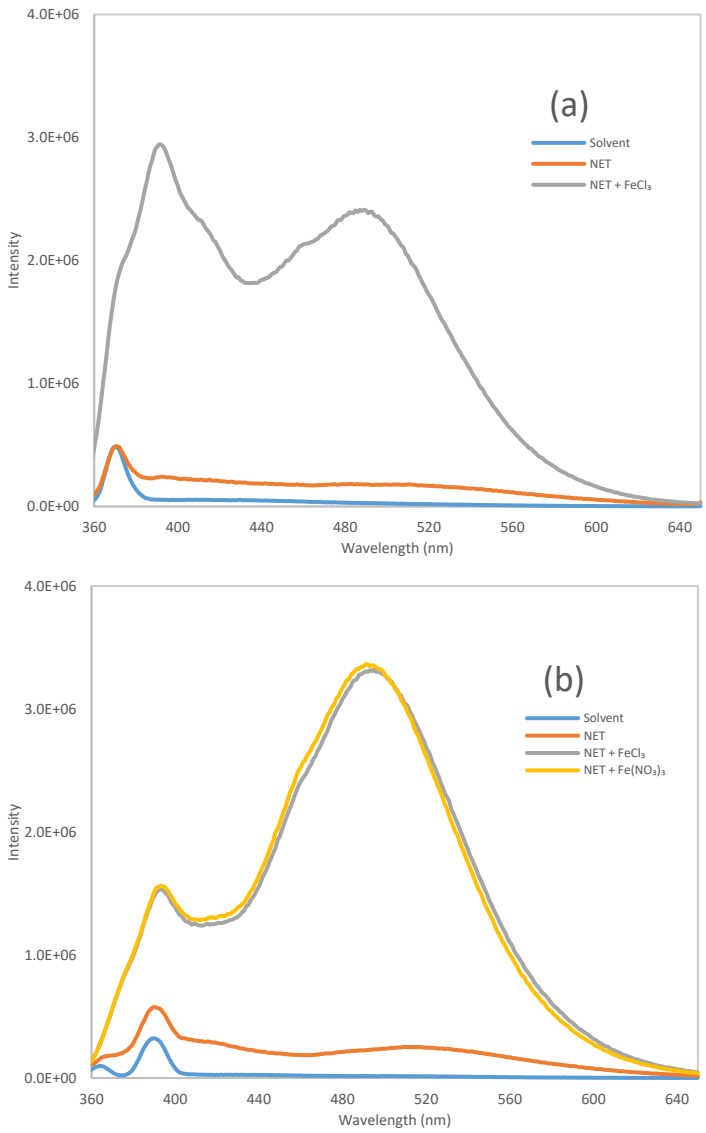

Figure 3.22: (a) Fluorescence emission spectrum of NET (10 µM) in 4:1 DMF/H_2O and with metal ions (100 µM) (λ_{ex}: 333 nm). (b) Fluorescence emission spectrum of NET (10 µM) in 2:3 DMF/H_2O and with metal ions (100 µM) (λ_{ex}: 346 nm).

3.4.3 Effect of pH on the Fluorescence of NET

The as prepared dye solution containing 10 μM NET in 2:3 DMF/H_2O has a pH of 6.2 while the same dye solution containing 100 μM $FeCl_3$ has a pH of 4.1. The fluorescence of 1,8-naphthalimide derivatives tend to have a strong pH dependance, with an observed increase in emission intensity at lower pH [14-16]. To explore the relationship between Fe^{3+} concentration, acidity, and fluorescence emission, samples with increasing $FeCl_3$ concentration were prepared. Each sample's fluorescence and measured pH are shown in Fig. 3.23. In Fig. 3.23 (a), the fluorescence spectra show the clear formation of the primary peak at 495 nm with increasing Fe^{3+} concentration. For each $FeCl_3$ concentration, the emission intensity at 495 nm and the measured pH are displayed in Fig. 3.23 (b). A linear relationship between iron concentration and emission intensity can be observed for the concentration range of 20-80 μM. With the initial additions of Fe^{3+}, the sample pH rapidly decreases, however, at higher concentrations of Fe^{3+}, the measured pH begins to level off. This effect may explain the apparent loss of linearity past 80 μM.

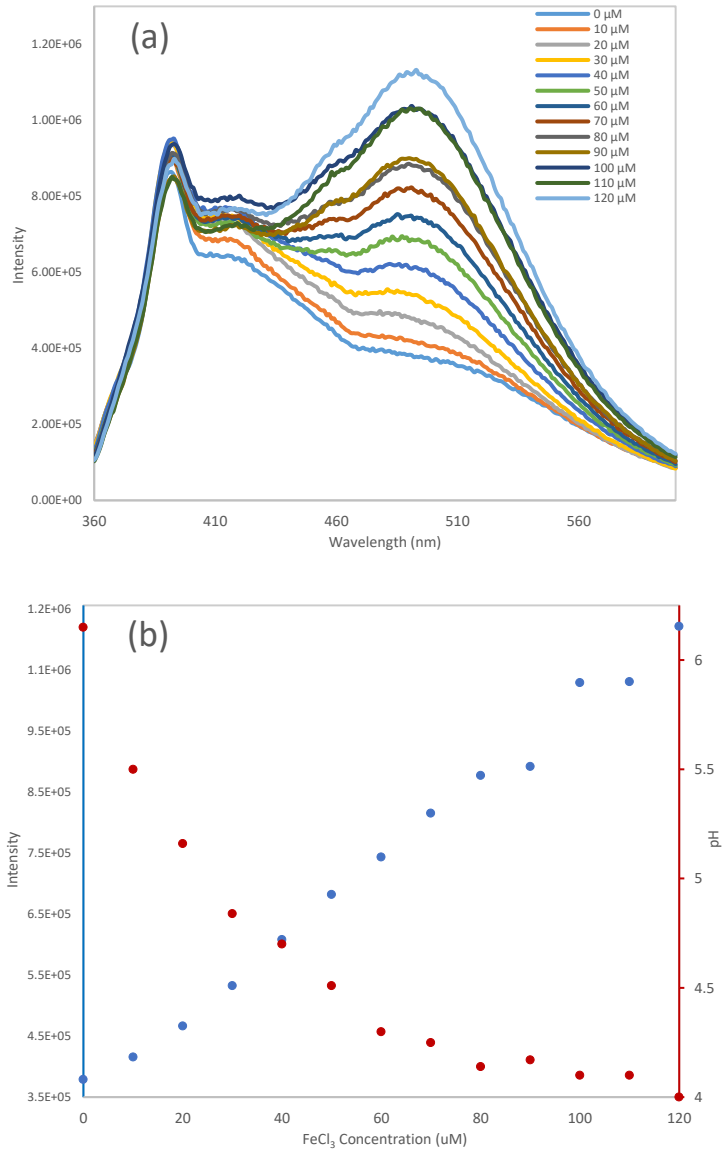

Figure 3.23: (a) Fluorescence emission spectrum of NET (10 µM) in 2:3 DMF/H_2O with increasing $FeCl_3$ concentration. (b) Comparing the effect of $FeCl_3$ concentration on emission intensity at λ_{em} = 495 nm (left axis) and solution pH (right axis).

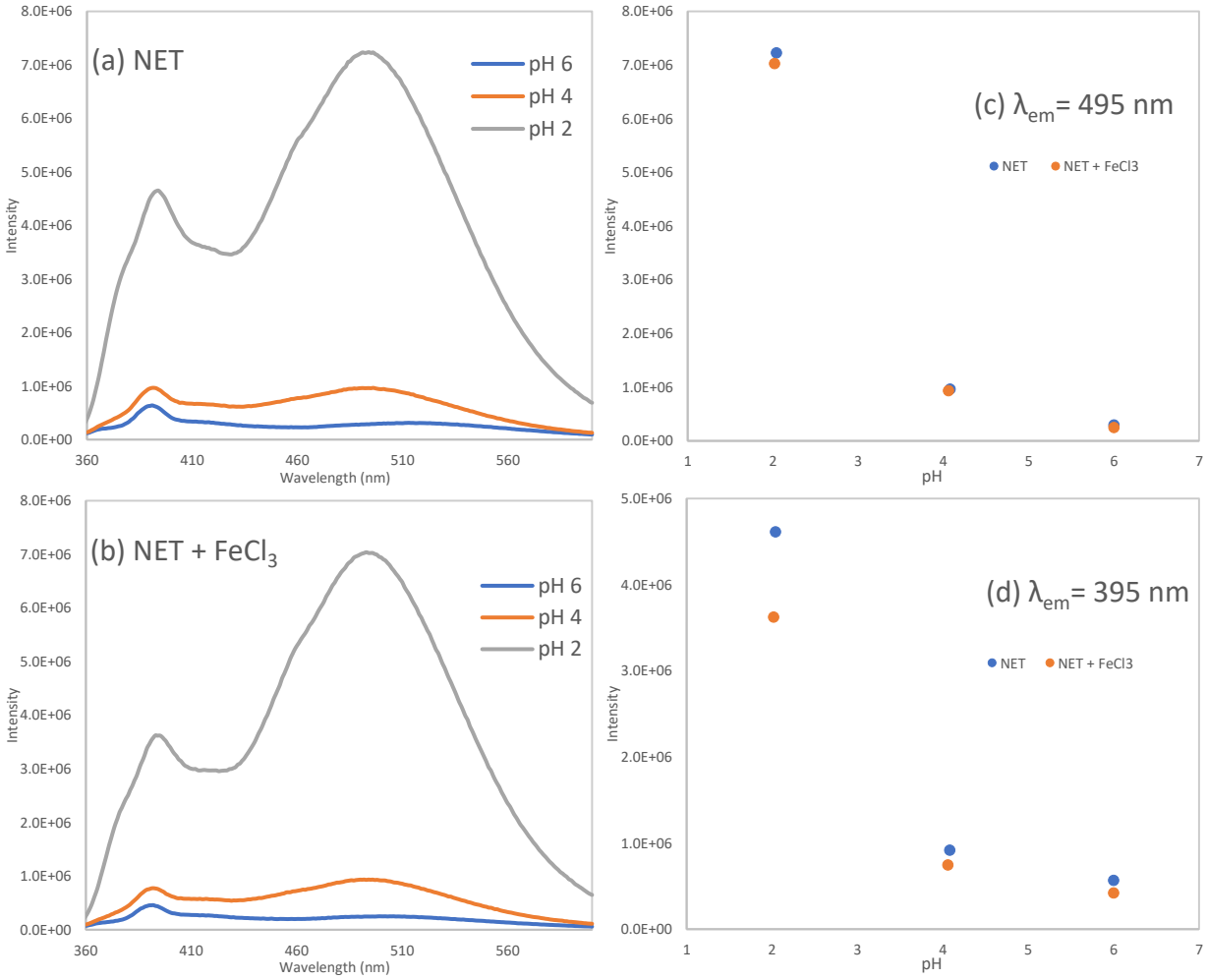

Figure 3.24: (a) Fluorescence emission of NET (10 μM) in 2:3 DMF/H_2O at differing pH. (b) Fluorescence emission of NET (10 μM) and $FeCl_3$ (100 μM) in 2:3 DMF/H_2O at differing pH. Emission intensity at (c) λ_{em} = 495 nm, and (d) λ_{em} = 395 nm, as a function of solution pH.

In order to further assess the effect of the acidity of the ferric salts in solution, controls were performed by measuring the fluorescence of the NET solution in 2:3 DMF/H_2O for pH adjusted to 2, 4, and 6 (Fig. 3.24 (a)) without Fe^{3+} ions present. Another set of data was collected with 100 µM $FeCl_3$ in solution and pH adjusted to 2, 3, and 6, as shown in Fig. 3.24 (b). When adjusted to the same pH, the samples containing $FeCl_3$ produced similar spectra to samples without any metal ions. This effect was seen with all three pH levels tested. Figs. 3.24 (c) and (d) show the emission intensity at 495 nm and 395 nm, respectively. For the primary peak at 495 nm, the intensities for both samples were similar for all pH levels. For the secondary peak at 395 nm, the intensities for the samples containing $FeCl_3$ were all consistently lower than the samples without. These results differ significantly from the data presented in the reported literature. In their paper, Yang, L., et al. shows a clear difference in intensity between NET samples with and without Fe^{3+} for the range of pH 3 through pH 7. However, we have reproduced this data several times and the effect reported by Yang, L., et al. could not be replicated when the pH of the solutions were adjusted to the same value for consistency.

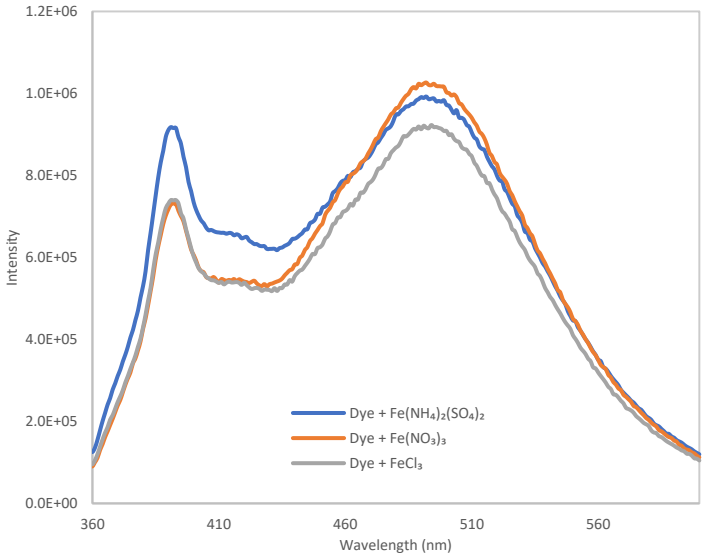

Figure 3.25: Fluorescence emission spectrum of NET (10 µM) in 2:3 DMF/H_2O with metal ions (100 µM) (λ_{ex}: 346 nm, pH 4).

To ensure the increased intensity is an effect of pH rather than cation identity, three more samples were prepared at pH 4, each containing $FeCl_3$, $Fe(NO_3)_3$, or $Fe(NH_4)_2(SO_4)_2$. The fluorescence spectra are displayed in Fig. 3.25. Like the previous results, both $FeCl_3$ and $Fe(NO_3)_3$ gave similar intensities. Both ferric iron salts produce the same pH level in solution, which can explain why their spectra in Fig. 3.22 (b) have the same intensity. At the same pH, the ferrous iron salt sample produced a spectrum with comparable shape and intensity to the ferric samples, providing further evidence that the fluorescence of NET is sensitive to pH and not Fe^{3+}.

The conclusion reported in the literature claims that NET behaves as a highly selecting "turn-on" fluorescent sensor for Fe^{3+} and claims that this high selectivity occurs in the pH range of 3.1-6.4. In this study, we have successfully synthesized and characterized NET, however, our results differ from those presented in the literature. The initial fluorescence testing of NET agreed with the literature results, but after further evaluation, NET shows no selectivity for Fe^{3+} when sample pH has been adjusted to the same level. Our results show that ion identity has no significant effect on the observed fluorescence of NET.

3.5 AMAE-RhB Dye

3.5.1 Synthesis and Characterization of AMAE-RhB Dye

2-(2-((anthracen-9-ylmethyl)amino)ethyl)-3',6'-bis(diethylamino)spiro[isoindoline-1,9'-xanthen]-3-one (AMAE-RhB) is reported by Jin et al. to selectively complex and fluoresce with Fe^{3+} [7]. In this work, the dye was synthesized according to the procedure outlined the literature. The synthesis consisted of three steps, with the formation of an intermediate precipitate (rhodamine b ethylenediamine). The identity of the intermediate was confirmed with ^1H NMR. The collected NMR spectrum of the intermediate matched the spectrum reported in the literature exactly with no evidence of impurity. The ^1H NMR spectrum of the final product, AMAE-RhB, is shown in Fig. 3.26. All peaks present in the collected spectrum match the NMR spectrum presented in the literature. The spectrum reported in the literature does show some irregularity, however. From 3.5-3.3 ppm, it appears that the spectrum was edited. This range can correspond to intensity from the presence of ethanol, which shows a quartet at 3.44 ppm in deuterated DMSO. Residual ethanol may have been left over from their synthesis; however, no explanation was given from the authors as to why the spectrum was edited. No peaks were observed in this range in our collected spectrum.

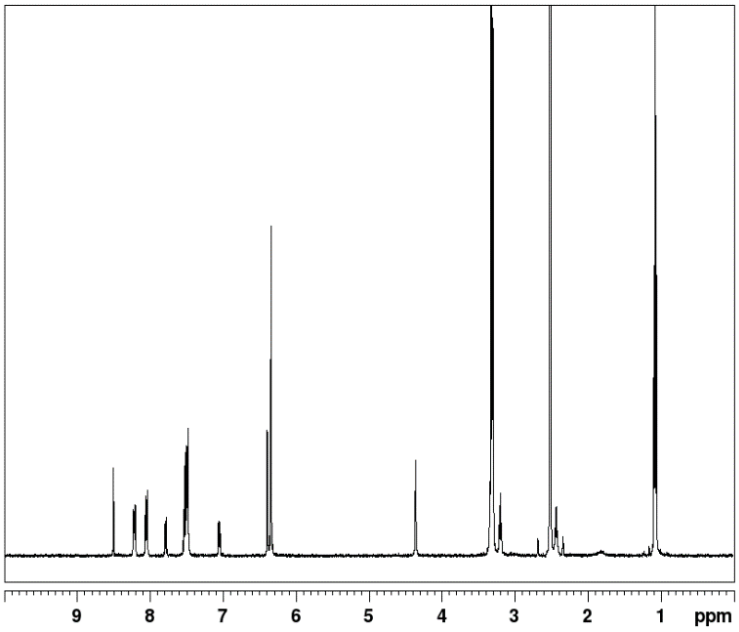

Figure 3.26: ^{1}H NMR spectrum of RhB Dye in DMSO-d_6.

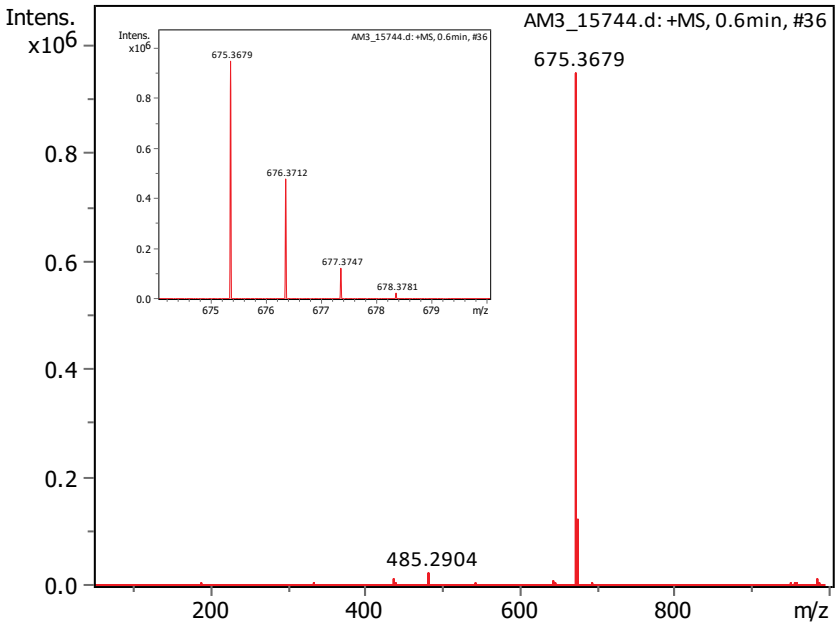

Figure 3.27: ESI mass spectrum of RhB Dye. The inset shows an expanded view of the molecular ion peak.

LC/MS was also conducted on the dye to confirm the synthesis. The mass spectrum of the AMAE-RhB dye is shown in Fig. 3.27, with the inset showing an expanded view of the molecular ion peak. A single large intensity is seen at 675.368 m/z, which corresponds to the RhB dye with a bound proton. A smaller peak is seen at 338.188 m/z (2.84%). This can be rationalized as being the RhB dye with two bound protons. Another small intensity can be seen at 485.291 m/z (5.68%). This mass value corresponds with the protonated intermediate compound. This intensity may come from an impurity, or it can come from fragmentation during ionization. The expanded molecular ion peak shows peaks at 675.3680 (100%), 676.3713 (50.54%), 677.3747 (13.21%), and 678.3782 (2.40%). These peaks match the expected isotopic pattern for the AMAE-RhB dye.

3.5.2 Fluorescence Emission Measurements of AMAE-RhB

Fluorescence measurements on the dye were performed using the parameters outlined in the literature. It was reported that the probe showed high selectivity towards Fe^{3+} in solution. Fig. 3.28 (a)-(c) show the fluorescence emission spectrums of RhB dye (10 μM) with and without an equivalent of $FeCl_3$. The exact concentration of the tris buffer used in the study was never stated so three different buffer concentrations were tested. Using 10 mM tris buffer as solvent, there was no difference in intensity in the samples with and without $FeCl_3$. The samples containing 1 mM tris showed a very slight increase in intensity with samples containing Fe^{3+}. With 0.1 mM tris buffer as solvent, a large fluorescence enhancement occurs at 585 nm when Fe^{3+} is present, indicating a potential emission enhancement due to the presence of Fe^{3+}.

With all three tested buffer concentrations, the spectrum of the sample without Fe^{3+} showed negligible change in its emission spectrum while the sample containing Fe^{3+} showed increasing intensity with decreasing buffer concentration. Due to the lowering buffer capacity yielding increased emission, it was suspected that the increase in intensity may have been due to pH sensitivity. Measuring the pH of both samples containing 0.1 mM buffer gave a pH of 6.85 for the sample without iron and a pH of 6 for the sample containing iron. New samples were prepared, adjusted to the same pH, and tested for their fluorescence. Fig. 3.29 (a) and (b) shows the fluorescence emission from these tests. At pH 6.85, the emission from the sample containing iron decreases and matches the sample without iron. A similar effect can be seen for the samples prepared at pH 6, where the emission from the sample without iron increases to a similar intensity as the sample containing iron. These results suggest that the RhB dye is more sensitive to pH than it is to the presence of Fe^{3+}.

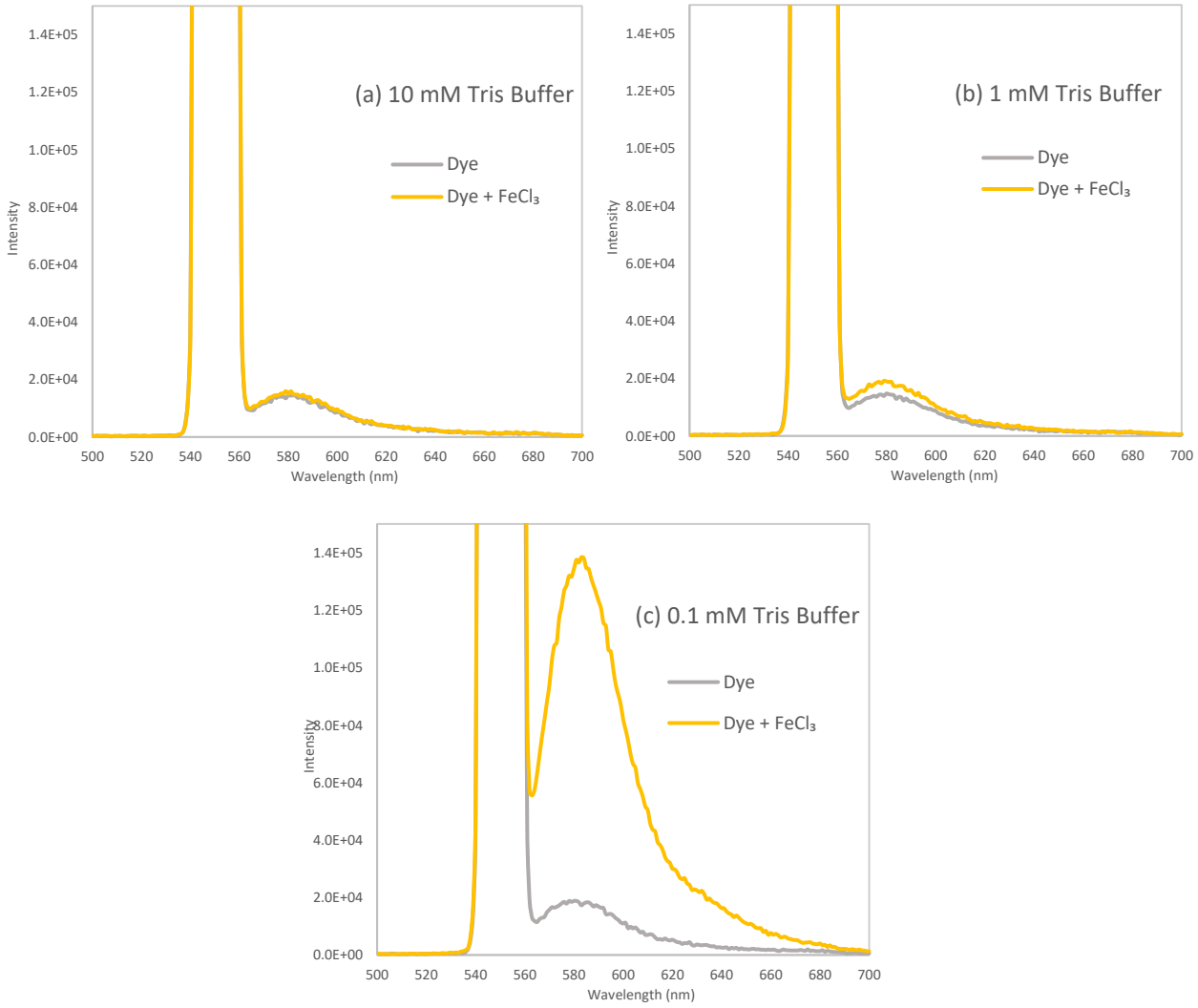

Figure 3.28: Fluorescence emission spectrums of RhB dye (10 µM) with and without $FeCl_3$ (10 µM) in (a) 10 mM, (b) 1 mM, and (c) 0.1 mM Tris-HCl buffer (1:9 EtOH/H_2O, pH 7)

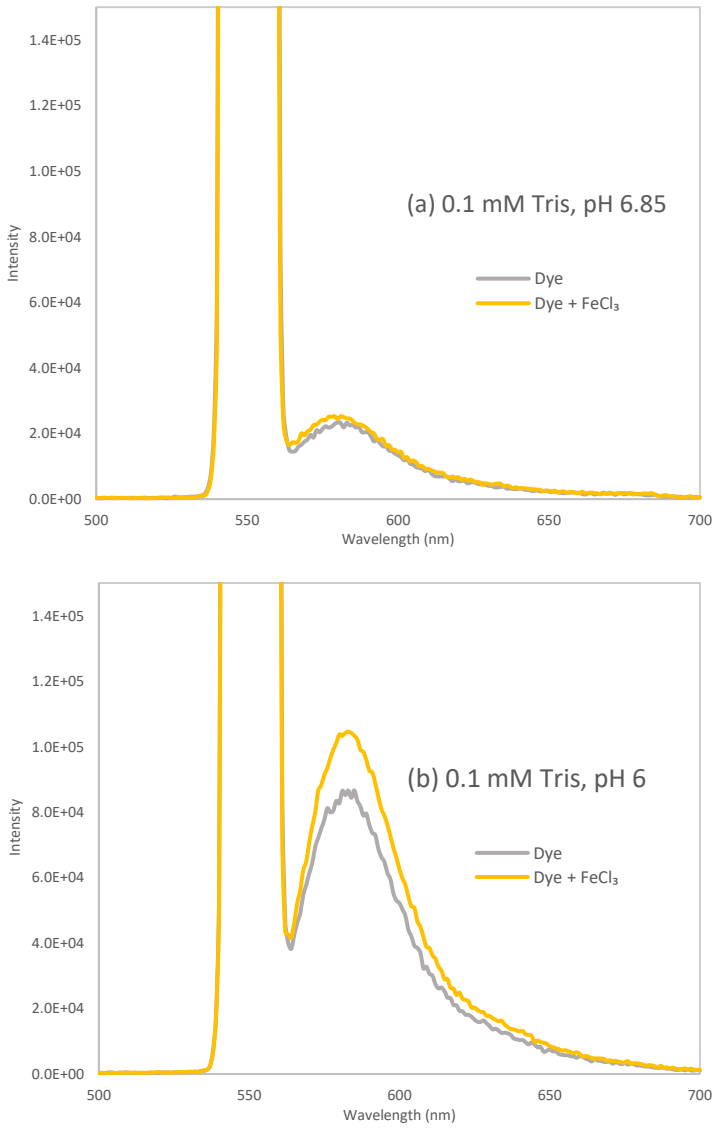

Figure 3.29: Fluorescence emission spectrums of RhB dye (10 µM) with and without $FeCl_3$ in Tris-HCl buffer (0.1 mM 1:9 EtOH/H_2O, pH 7) adjusted to (a) pH 6.85 and (b) pH 6 (λ_{ex} = 550 nm).

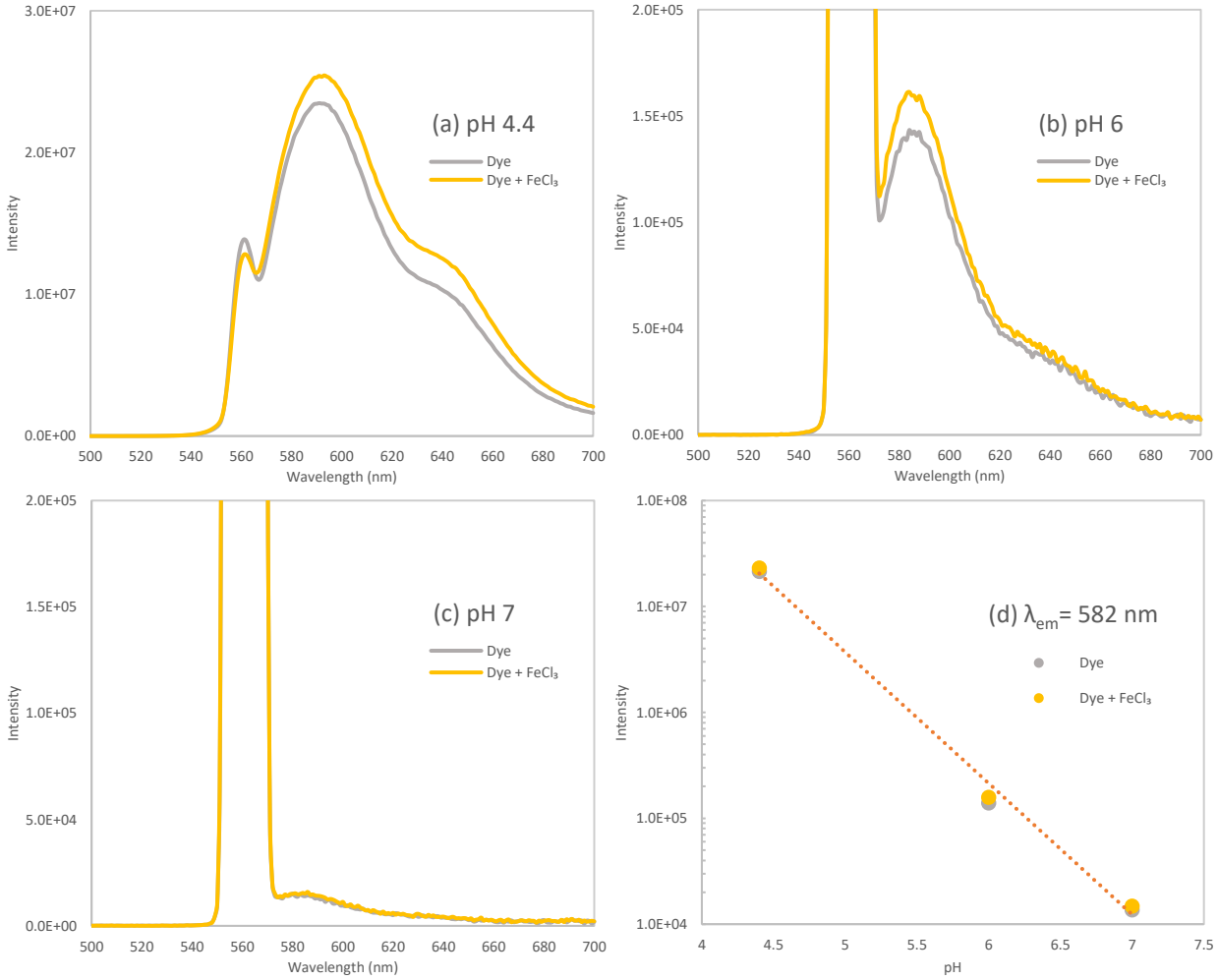

Figure 3.30: Fluorescence emission spectrums of RhB dye (10 µM) with and without $FeCl_3$ (10 µM) in Tris-HCl buffer (10 mM, 1:9 EtOH/H_2O, pH 7) adjusted to (a) pH 4.4, (b) pH 6 and (c) pH 7 (λ_{ex} = 560 nm). (d) shows the emission at 590 nm from these samples plotted against sample pH.

3.5.3 Effect of pH on the Fluorescence of AMAE-RhB

To further confirm the lack of Fe^{3+} sensitivity, fluorescence testing was repeated with an expanded pH range. Samples were prepared at pH 4.4, pH 6, and pH 7. Their fluorescence spectra are displayed in Fig. 3.30 (a)-(c). For the three pH values tested, both samples with and without Fe^{3+} have similar emission, with emission intensity increasing significantly with increasing acidity. Fig. 3.30 (d) shows the intensity at 590 nm for each sample. A near logarithmic relationship is observed between intensity and pH for the pH range tested. For samples at pH 4.4 and pH 6, samples containing Fe^{3+} gave slightly greater intensities than samples without, however, the observed fluorescence does not match what was reported in the original study. The authors claim that samples containing Fe^{3+} should give higher emission intensity for pH levels under pH 8, while giving a maximum difference in intensity between pH 5 and pH 7. This effect was not observed in any tests performed.

The authors also claim that the RhB dye shows no fluorescence emission for pH 2 though pH 12. Fig. 3.31 (a) shows the fluorescence spectra for RhB dye adjusted to a range of different pH values while (b) shows the 589 nm emission intensity for each pH value. RhB dye shows no intensity for each basic pH tested. Starting at pH 7, the emission intensity begins to increase, reaching a maximum value near pH 3.5. Samples between pH 3 and pH 4 visibly become vibrant pink under normal room lighting. This color change was not affected by changing the identity of the solvent.

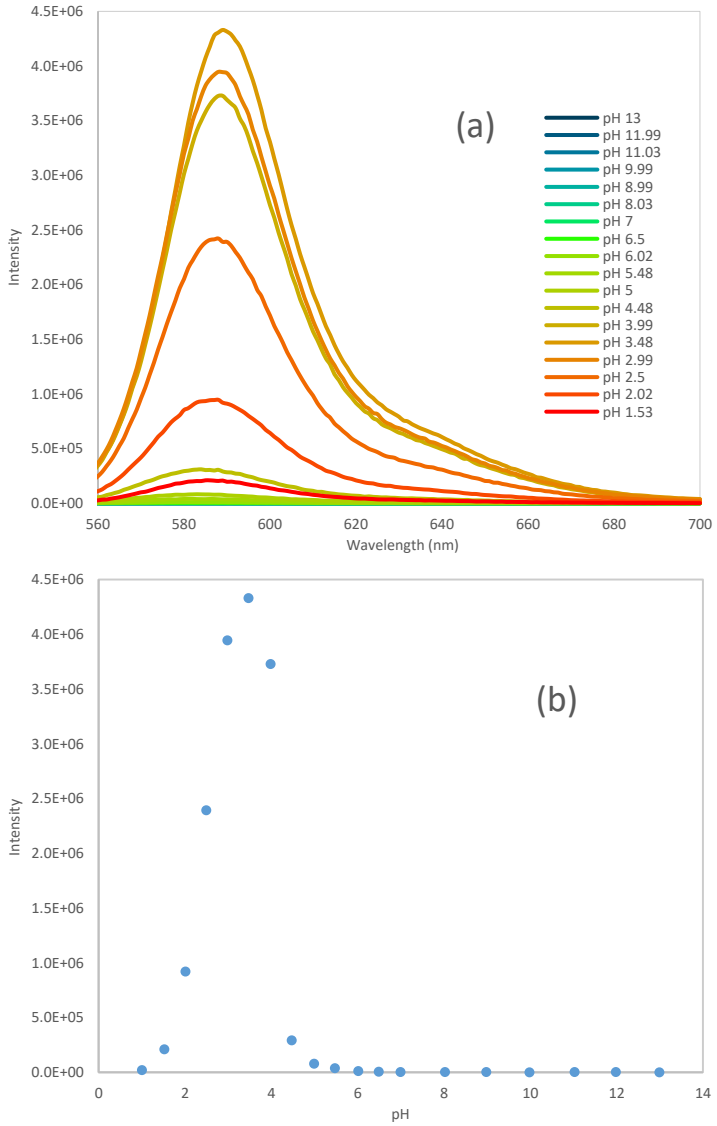

Figure 3.31: (a) Fluorescence emission spectrums of RhB dye (10 μM) in Tris-HCl buffer (10 mM, 1:9 EtOH/H_2O, pH 7) at different pH. Emission intensity at 589 nm is plotted against pH in (b).

4. Conclusions and Future Work

The goal of this proposed work is to demonstrate a chemical tag selective to Fe^{2+} and Fe^{3+} for detecting internal corrosion of a gas pipelines. We have successfully identified an Fe^{2+} dye, FerroFarRed, that is highly selective to Fe^{2+}, very stable across a wide range of pH range, and commercially available. The Fe^{3+} dye, however, is not commercially available. We have therefore setout to synthesize reported dye molecules that are selectively to Fe^{3+}. These are the (1) (E)-N-(1H-benzo[d]imidazol-2-yl)-1-(quinolin-2-yl)methanimine (BIM), (2) N-[Tris(N-ethyl-1,8-naphthalimide)]amine (NET), and (3) 2-(2-((anthracen-9-ylmethyl)amino)ethyl)-3',6'-bis(diethylamino)spiro[isoindoline-1,9'-xanthen]-3-one (AMAE-RhB).

Each potential fluorescent tag was synthesized according to the listed procedure in its respective literature. The NET and AMAE-RhB dyes were successfully synthesized with little to no impurity, as evidenced by the collected characterization data. The reported synthetic procedure for the BIM dye did not yield a precipitate. A modified procedure was used to synthesize a precipitate of the BIM dye. The identity of the dye was confirmed using ^1H NMR Spectroscopy and ESI Mass Spectrometry. While there is evidence of impurity in the BIM precipitate, the collected data shows that the target BIM molecule is present in the precipitate.

Once synthesized, each dye was tested for their fluorescence in the presence of Fe^{3+} and other metal ions. While the initial results for each dye were promising, upon further testing, a trend of pH dependance was observed for each dye. Of the metal ions tested, Fe^{3+} exhibited the highest acidity. When compared to samples with other metal ions present, Fe^{3+} containing samples gave the highest fluorescence intensity. However, when the pH of the samples were all adjusted to the same value, the observed intensity of samples containing Fe^{3+} becomes the same as the samples without ions. This effect was observed for all three dyes at multiple different pH values.

Further testing showed a clear increase in fluorescence emission at acidic pH for each dye, independent of the presence of Fe^{3+}, with each dye showing little to no emission at $pH \geq 7$. This observed trend is inconsistent with the pH data reported in the literature for the NET and AMAE-RhB dyes. The literature for the BIM dye did not report any data on pH past mentioning that a 1 mM HEPES buffer at pH 7.3 was used for testing. BIM was reported to give increased intensity in the presence of Cr^{3+} and Al^{3+} cations. Both cations gave increased intensity in our testing as well due to their increased acidity compared to the other metal cations tested. Also, from our results for the AMAE-RhB dye, a 1 mM buffer does not provide enough buffer capacity to correct for the acidity from Fe^{3+}, although the sample preparation for the AMAE-RhB and

BIM testing were not completely analogous so they should not be directly compared.

It is unknown why there are such major discrepancies between our collected data and the data reported in the literature. Our fluorescence testing methodology was matched to what was reported in the literature. It is possible some necessary details were omitted, such as the missing concentration of the tris buffer in the literature for the AMAE-RhB dye. With regards to the observed discrepancies, nothing conclusive can be said past that we do observe a direct correlation between fluorescence intensity and pH and no correlation is observed between intensity and the presence of Fe^{3+}.

In order to continue this project in the future, several other Fe^{3+} selective dyes have been considered. A Schiff base reported by Faizi et. al. reportedly shows high fluorescence selectivity towards Fe^{3+}, with a maximum emission intensity at 610 nm using an excitation wavelength of 395 nm [17]. We synthesized this dye according to the reported procedure; however, preliminary fluorescence testing did not match the reported data.

You et. al. reports another Fe^{3+} selective rhodamine-based dye that shows some promise as a potential Fe^{3+} fluorescent tag [18]. In the presence of Fe^{3+}, the dye has a reported maximum emission intensity centered at 585 nm when excited with 500 nm light. Data on the fluorescence emission as a function of pH is also reported. The dye is extremely selective for Fe^{3+} in the pH range of 4-9.

Another dye that was promising initially is reported by Wei et. al.[19]. It is also a rhodamine-based dye that is reported to selectively fluoresce in the presence of Fe^{3+} at a maximum emission intensity of 559 nm using an excitation wavelength of 500 nm. Fe^{2+} also gives increased intensity; however, the intensity from Fe^{3+} is an order of magnitude greater. Data on the fluorescence intensity as a function of pH is provided in the supplementary information section. Samples were prepared in a 10 mM acetonitrile/Tris HCL buffer at pH 7.3. In the experimental section, they report dissolving Fe^{3+} and Fe^{2+} salts in 0.01 M HCl. The other metal salts were dissolved in double distilled water. No explanation was given as to why only these two metal salts were dissolved in acid. Samples containing Fe^{3+} and Fe^{2+} were the only samples that gave a reported increase in intensity.

Studies that focus on ion selective fluorophores should have a more rigorous understanding of the role of pH on their dye's fluorescence, as exemplified by our results. Due to the typical pH dependance on a dye's fluorescence, Fe^{3+} and other acidic metal cations can give the illusion of selectivity during initial characterization. A thorough investigation into the role of

pH should be provided whenever a claim of selectivity is made to ensure an accurate conclusion is drawn.

Unfortunately, due to the unforeseen circumstances directly or indirectly affected by the pandemic, we were not able to complete the pressure and flow test intended for this project. We have several conversations with DNVGL regarding the pressure tests and have provided a set of FerroFarRed samples to test the Fe^{2+}-FerroFarRed response to pressure. We have instead pivoted to investing the chemical nature of the reported Fe^{3+} dye that has proven to be quite interesting. We still think that it would be interesting to pursue additional pressure and flow test of the Fe2+ complex and also the pressure, flow and temperature test of the pH sensitive dyes investigated over the duration of this work.

5. References

1. Hirayama, T.; Tsuboi, H.; Niwa, M.; Miki, A.; Kadota, S.; Ikeshita, Y.; Okuda, K.; Nagasawa, H. A Universal Fluorogenic Switch for Fe(ii) Ion Based on N-Oxide Chemistry Permits the Visualization of Intracellular Redox Equilibrium Shift towards Labile Iron in Hypoxic Tumor Cells. Chemical Science **2017**, 8 (7), 4858–4866.

2. Kar, C.; Samanta, S.; Mukherjee, S.; Datta, B. K.; Ramesh, A.; Das, G. A Simple and Efficient Fluorophoric Probe for Dual Sensing of Fe^{3+} and F−: Application to Bioimaging in Native Cellular Iron Pools and Live Cells. New J. Chem. **2014**, 38 (6), 2660–2669.

3. Yang, L.; Yang, W.; Xu, D.; Zhang, Z.; Liu, A. A Highly Selective and Sensitive Fe^{3+} Fluorescent Sensor by Assembling Three 1,8-Naphthalimide Fluorophores with a Tris(Aminoethylamine) Ligand. Dyes and Pigments **2013**, 97 (1), 168–174.

4. Zhao, L. Y.; Mi, Q. L.; Wang, G. K.; Chen, J. H.; Zhang, J. F.; Zhao, Q. H.; Zhou, Y. 1,8-Naphthalimide-Based 'Turn-on' Fluorescent Sensor for the Detection of Zinc Ion in Aqueous Media and Its Applications for Bioimaging. Tetrahedron Letters **2013**, 54 (26), 3353–3358.

5. Fu, Y.; Li, P.; Kang, J.-X.; Liu, X.-Y.; Li, G.-Y.; Ye, F. A Novel 1,8-Naphthalimide Derivative as an Efficient Silver(i) Fluorescent Sensor. Journal of Luminescence **2016**, 178, 156–162.

6. Yordanova-Tomova, S.; Cheshmedzhieva, D.; Stoyanov, S.; Dudev, T.; Grabchev, I. Synthesis, Photophysical Characterization, and Sensor Activity of New 1,8-Naphthalimide Derivatives. Sensors **2020**, 20 (14), 3892.

7. Jin, X.; Wang, S.; Yin, W.; Xu, T.; Jiang, Y.; Liao, Q.; Xia, X.; Liu, J. A Highly Sensitive and Selective Fluorescence Chemosensor for Fe^{3+} Based on Rhodamine and Its Application in Vivo Imaging. Sensors and Actuators B: Chemical **2017**, 247, 461–468.

8. Dujols, V.; Ford, F.; Czarnik, A. W. A Long-Wavelength Fluorescent Chemodosimeter Selective for Cu(Ii) Ion in Water. Journal of the American Chemical Society **1997**, 119 (31), 7386–7387.

9. Jiao, Y.; Zhang, L.; Zhou, P. A Rhodamine B-Based Fluorescent Sensor toward Highly Selective Mercury (II) Ions Detection. Talanta **2016**, 150, 14–19.

10. Sunnapu, O.; Kotla, N. G.; Maddiboyina, B.; Asthana, G. S.; Shanmugapriya, J.; Sekar, K.; Singaravadivel, S.; Sivaraman, G. Rhodamine Based Effective Chemosensor for

Chromium(Iii) and Their Application in Live Cell Imaging. Sensors and Actuators B: Chemical **2017**, 246, 761–768.

11. Leng, X.; Xu, W.; Qiao, C.; Jia, X.; Long, Y.; Yang, B. New Rhodamine B-Based Chromo-Fluorogenic Probes for Highly Selective Detection of Aluminium(III) Ions and Their Application in Living Cell Imaging. RSC Advances **2019**, 9 (11), 6027–6034.

12. Incident statistics. https://www.phmsa.dot.gov/hazmat-program-management-data-and-statistics/data-operations/incident-statistics (accessed Aug 20, 2022).

13. Pipeline pigging . https://www.pipingengineer.org/pipeline-pigging/ (accessed Aug 20, 2022).

14. Grabchev, I.; Qian, X.; Xiao, Y.; Zhang, R. Novel Heterogeneous Pet Fluorescent Sensors Selective for Transition Metal Ions or Protons: Polymers Regularly Labelled with Naphthalimide. New Journal of Chemistry **2002**, 26 (7), 920–925.

15. Yordanova, S.; Stoianov, S.; Grabchev, I.; Petkov, I. Detection of Metal Ions and Protons with a New Blue Fluorescent Bis(1,8-Naphthalimide). International Journal of Inorganic Chemistry **2013**, 2013, 1–6.

16. Staneva, D.; Bosch, P.; Asiri, A. M.; Taib, L. A.; Grabchev, I. Studying PH Dependence of the Photophysical Properties of a Blue Emitting Fluorescent Pamam Dendrimer and Evaluation of Its Sensor Potential. Dyes and Pigments **2014**, 105, 114–120.

17. Faizi, M. S.; Gupta, S.; Mohan K., V.; Jain, V. K.; Sen, P. Highly Selective Visual Detection of Fe^{3+} at PPM Level. Sensors and Actuators B: Chemical **2016**, 222, 15–20.

18. You, Q.-H.; Huang, H.-B.; Zhuang, Z.-X.; Wang, X.-R.; Chan, W.-H. A New Rhodamine-Based Fluorescent Probe for the Discrimination of Fe^{3+} from Fe^{2+}. Bulletin of the Korean Chemical Society **2016**, 37 (11), 1772–1777.

19. Wei, Y.; Aydin, Z.; Zhang, Y.; Liu, Z.; Guo, M. A Turn-on Fluorescent Sensor for Imaging Labile Fe^{3+} in Live Neuronal Cells at Subcellular Resolution. ChemBioChem **2012**, 13 (11), 1569–1573